

**Post-Laramide Exhumation and Topography in the Madison and
Gallatin Ranges of Southwest Montana from Apatite (U-Th)/He
Thermochronometry**

A Thesis

Presented in Partial Fulfillment of the Requirements for the

Degree of Master of Science

with a

Major in Geology

in the

College of Graduate Studies

University of Idaho

by

Chloë Weeks

Approved by:

Major Professor: Jessica R. Stanley, Ph.D.

Committee Members: Elizabeth J. Cassel, Ph.D.; Marissa Tremblay, Ph.D.

Department Administrator: Alistair MS Smith, Ph.D.

AUGUST 2022

Abstract

Since the end of the Laramide Orogeny, southwest Montana has been subject to a complex array of tectonic, volcanic, and mantle dynamic processes that have left an imprint on the topography and landscape. Here, we aim to examine the impact of post-orogenic and more recent hotspot-related processes on the landscape by quantifying the Cenozoic exhumation history of the Madison and Gallatin Ranges, located on the northern flank of the Yellowstone hotspot in southwest Montana. We apply the apatite (U-Th)/He (AHe) low-temperature thermochronometer to Cretaceous and Tertiary intrusions found throughout the area to provide constraints on the Cenozoic cooling history. We acquired AHe dates from bedrock samples collected along two elevation transects and one horizontal transect to establish any differences in exhumation rates and magnitudes. AHe dates from 16 samples produced a range of dates from 70 ± 3.4 Ma to 6.4 ± 0.28 Ma. Samples of the largest elevation transect display a positive relationship between date and elevation suggesting they are undergoing continuous exhumation at either a constant or increasing relief during the Eocene through Oligocene. Increased topography and erosion during Eocene extension and eventual extensional collapse may have driven exhumation and cooling during this time, in addition to increased topography and erosion from the widespread magmatism of the Absaroka Volcanic Province. Changes to topography may be attributed to surface uplift, increasing relief, or a combination of the two. Signals of later cooling in samples close to the Madison Fault are inferred to predominantly record fault driven exhumation. Erosional exhumation due Yellowstone hotspot driven regional uplift appears to be minimal.

Acknowledgments

Rarely is anything truly accomplished alone. Despite our own capabilities, it is those around us who help us achieve our goals through their support and faith in not only our abilities, but also our potential.

Firstly, I would like to recognize the organizations and people that have supported this project. I appreciate The Tobacco Root Geological Society, The Colorado Scientific Society, and GSA for grants that will help improve and present this work. Thanks to the team at GeoSeeps Services, Jim McMillan and Victoria, for your help processing my samples and all the laughs. Thanks to Renee Jensen-Hasfurther for making sure our department runs smoothly and always looking out for us graduate students. Many thanks to my committee member Dr. Marissa Tremblay for her time, valuable comments, and counsel throughout this project.

To my fellow graduate students, thank you for the support and friendship you've shown me throughout my time here, particularly during the pandemic when it was especially difficult to socialize and find that elusive work-life balance. A special shout out to Haley Thoresen and McKayla Meier whose support and friendship have made my graduate school experience meaningful. I look forward to our continued slack chats, catching up at conferences, and watching you both cultivate incredible careers as badass geologists. Special thanks to Dr. Liz Cassel – you poetic, noble land mermaid – for all the classes, laughs, and insight. You helped push me to think harder and be a better scientist.

Lastly and most importantly, all my gratitude to my advisor Dr. Jessica Stanley whose patient and thoughtful guidance reminds me that I am capable of more than I give myself credit for. I've gained a new appreciation for my own curiosity from your mentorship, I am thankful to have found an advisor that believes in me and my potential like you do. There are too many laughs and moments to mention; I am grateful for the chance to be your student.

Dedication

None of this would be possible without the people that believe in me and show me dreams are worth chasing. I am grateful to my Cordier family for their constant support and love. Thanks to my dad for always supporting me and reminding me how important it is to love what you do. To Charlie for his encouragement, without whom I would be nothing.

This accomplishment is dedicated to my grandpa who took pride in all my endeavors.

Table of Contents

Abstract	ii
Acknowledgments	iii
Dedication	iv
List of Tables	vi
List of Figures	vii
Introduction	1
Background	3
Geologic Background of Western US	3
Tectonics, Topography, and Magmatism in Southwest Montana	6
(U-Th)/He Thermochronometry	8
Methods	9
Strategy and Samples	9
Apatite (U-Th)/He Methods	11
Thermal History Modeling Methods	12
Results	15
Inverse Modeling Results	24
Discussion	25
Post-Laramide Cooling in the Northern Madison and Gallatin Ranges	25
Paleocene Cooling	29
Madison Fault Driven Exhumation	35
Yellowstone Hotspot Influence on Cooling	37
Conclusions	40
Future Work and Outstanding Questions	41
References	44

List of Tables

Table 1 Apatite (U-Th)/He data from southwest Montana.....	17
Table 2 Thermal history model inputs for southwest Montana samples	14

List of Figures

Figure 1 Regional terrain map of southwest Montana, eastern Idaho and northwest Wyoming with an inset map showing the northwest region of the United States and relevant geological features.....	3
Figure 2 Simplified geologic map of our study area with sample localities	11
Figure 3 (A-E) AHe eU and thermal modeling results for all samples in the Gallatin Gateway transect	20
Figure 4 (A-E) AHe eU and thermal modeling results for all samples in the Big Sky transect.....	21
Figure 5 (A-D) AHe eU and thermal modeling results for all samples in the Madison Range transect	22
Figure 6 Average AHe cooling dates plotted against elevation for all three transects.....	23
Figure 7 Average AHe cooling dates for the Madison Range and Big Sky transects plotted against distance from the Madison Fault.....	24
Figure 8 (A-C) Kernel density estimate (KDE) plots of AHe cooling dates for the Gallatin Gateway, Big Sky and Madison Range transects.....	29
Figure 9 Timeline diagram depicting generalized major geologic events within the Cordillera Orogenic system.....	32

Introduction

The processes that govern the evolution of continental topography, including tectonics, lithospheric processes, mantle dynamics, and erosion, are uniquely interconnected and create compelling and complex geological systems. The Cenozoic history of plate motions and mantle dynamics along the western United States have shaped an intricate history of deformation and magmatism within the North American Cordillera. Contractional stress that gave rise to the Sevier and Laramide Orogenies transitioned to extensional stress during the early Eocene resulting in deformation and magmatism that greatly impacted topography throughout regions within and near the fold and thrust belt (e.g., Constenius, 1996, Janecke, 2007). The addition of deformation and magmatism along the migratory path of the Yellowstone hotspot has caused overprinting and reactivation of both Sevier and Laramide aged structures, further contributing to changes to topography and landscape evolution (Anders and Sleep, 1992; Janecke, 2007).

Changes to surficial processes from the Yellowstone hotspot (YSH) is important to understanding the mantle driven processes below the surface. Such an example of dynamic topography is the doming of the surface that occurs at and surrounding intraplate hotspots such as the Yellowstone hotspot (YSH) (Waschbusch and McNutt, 1994; Sears and Thomas, 2007; Smith et al, 2009). The YSH has long fueled studies across the western US and its long-lived history has influenced a plethora of events since its inception. The most accepted hotspot model favors a mantle plume origin, although there is some debate on the depth of the plumes root (e.g., Pierce and Morgan, 2009; Camp and Wells, 2021, and references therein). Morgan (1972) first introduced the concept of a stationary mantle plume which “migrates” with movement of the overriding lithosphere. The migration of a plume of this magnitude creates a pattern of uplift and high topography referred to as the Yellowstone Crescent of High Terrain (YCHT) (Anders and Sleep, 1992). This parabola shaped region of high topography is accompanied by active deformation and seismicity on each side with an aseismic region of subsidence towards the center (Anders et al., 1989; Fritz and Sears, 1993). Studies of the hotspot’s eastward migration and progression across North America have led to a greater

understanding of plume-lithosphere interactions and deformation. Improved insight into the effects of hotspot processes on landscape evolution is valuable for understanding drivers of topographic change and mantle-surface connections.

The northern rim of the active manifestation of the YSH within the YCHT is an ample location to study hotspot evolution and focus on landscape development closer to the hotspot source. Southwest Montana lies within this northern region of the YCHT and its proximity to an actively evolving hotspot makes it an ideal location to investigate how mantle processes are actively impacting topography on the surface. Specifically, the Gallatin River Valley of southwest Montana includes the Gallatin and Madison Ranges just east of the Sevier fold and thrust belt in the Laramide foreland (Fig. 1). Previous studies have investigated the tectonothermal history of this region using apatite and zircon fission track and AHe thermochronology, but their data and interpretations were focused on Laramide and earlier thermal histories that pre-date the arrival and progression of the hotspot (Carrapa et al., 2019; Kaempfer et al., 2021).

The Madison and Gallatin Ranges, including the Gallatin River Valley, were subject to magmatism during Laramide compression, as evidenced by Tertiary-Cretaceous aged intrusives throughout the region (Garihan et al., 1983; Tysdal et al., 1986; Kellogg and Williams, 1998; Vuke et al., 2002). Their age of emplacement (69 ± 1 Ma, Tysdal, 1986) makes them potentially resourceful recorders of post-Laramide exhumation. This study uses apatite low temperature apatite (U-Th)/He (AHe) thermochronometry to quantify the magnitude of Cenozoic landscape evolution on the northern flank of high topography surrounding the YSH to quantify the impact of post-Laramide processes, including the approach of the YSH to its current location on exhumation and/or relief in the region. The lower temperature sensitivity of the AHe system applied to these intrusive lithologies, which record shorter thermal histories than surrounding rocks, may be able to isolate lower magnitude exhumation after the events of the Laramide. Our new AHe data attempts to find links between hotspot surficial processes and periods of post-Laramide cooling in addition to identifying any

supplementary drivers of exhumation within the larger history of landscape evolution in southwest Montana.

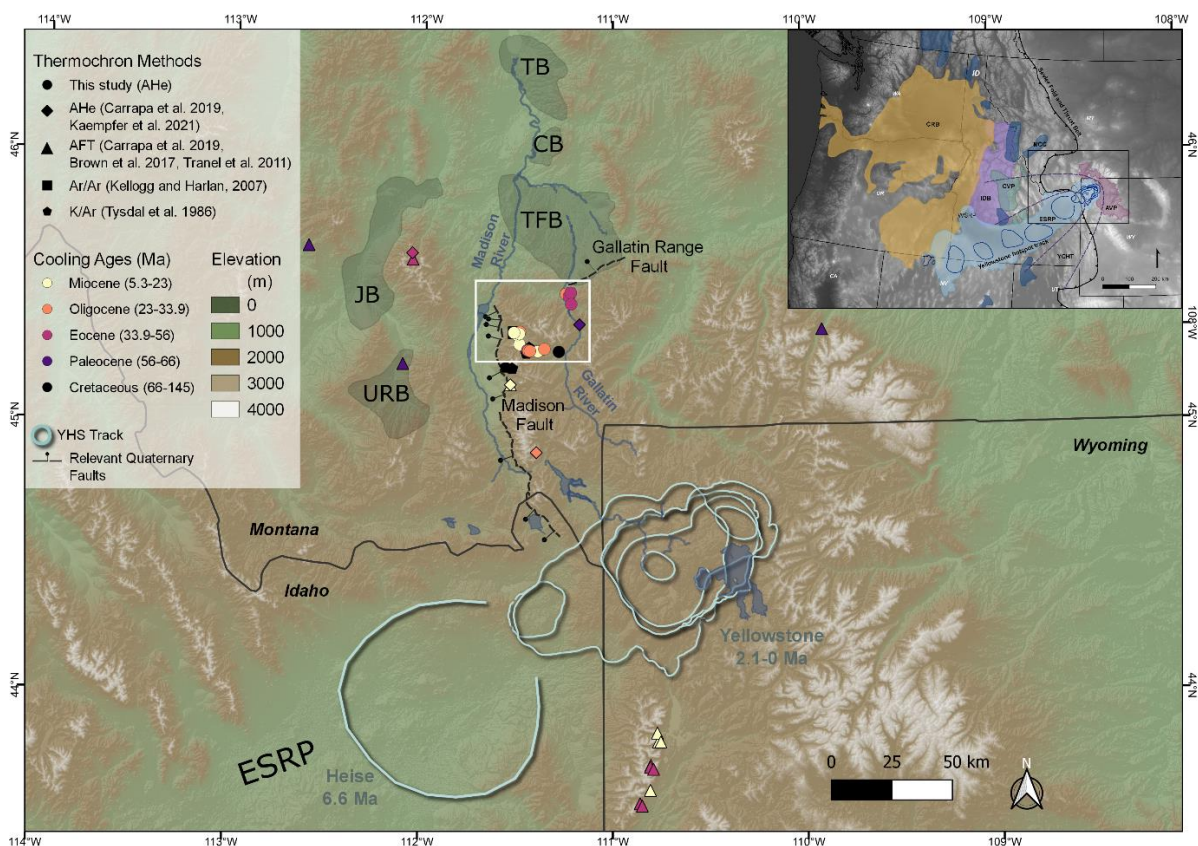


Fig. 1: Regional terrain map of southwest Montana, eastern Idaho and northwest Wyoming. The inset map shows the northwest region of the United States with highlighted provinces (AVP – Absaroka Volcanic Province, CRB – Columbia River Basalts, CVP – Challis Volcanic Province, ESRP – Eastern Snake River Plain, IDB – Idaho Batholith, YCHT – Yellowstone Crescent of High Terrain, WSRP – Western Snake River Plain), a generalized boundary of the Sevier Fold and Thrust Belt, and a black box indicating the area of Figure 1. The study area (white box) includes the Northern Madison and Gallatin Ranges. Color symbols indicate the location and cooling dates from this study and previously published thermochronology studies. Other major features include the Eastern Snake River Plain (ESRP), the track of the Yellowstone Hotspot (YHS Track), the Madison and Gallatin Range Faults and basins of interest north and northwest of the study area (CB – Clarkston Basin, JB – Jefferson Basin, TB – Townsend Basin, TFB – Three Forks Basin, URB – Upper Ruby Basin).

Background

Geologic Background of Western US

Our study region in southwest Montana (Fig. 1) sits within the North American Cordillera orogenic system, which extends through >6000 km of North America from Central Mexico to the Alaskan and Canadian Arctic. Eastward subduction of the oceanic Farallon and Kula plates beneath the North American plate resulted in inboard deformation that initiated during the Jurassic to

Paleogene, with continued subduction to the present off the coast of the Pacific Northwest and along the western coast of North America (e.g., DeCelles, 2004; Dickinson, 2004; Yonkee and Weil, 2015). Within the US portion of the Cordillera, initiation of crustal shortening began in the mid-late Cretaceous with thin-skinned Sevier deformation. The mid-Cretaceous also gave rise to the extensive Idaho Batholith, which produced magmatism between ~98-54 Ma into ancestral North American crust with late-stage magmatism extending into parts of western Montana (Janecke, 2007; Gaschnig et al., 2010). A decrease in subduction angle from ~80-40 Ma resulted in thick-skinned Laramide deformation characterized as basement block uplifts, and was partly coeval with the tail end of the Sevier Orogeny (e.g., Dickinson et al., 1988). Despite extensive deformation during this period, the Laramide produced little magmatism and was considered largely amagmatic (Chetel et al., 2011; Carrapa et al., 2019).

The tectonic regime within the Cordillera transitioned from contractional to extensional in the Cenozoic as evidenced by nearly overlapping periods of magmatism and unroofing (Janecke, 1992; Constenius, 1996; O'Neill et al., 2004; Janecke, 2007). The timing of this transition varies along the length of the Cordillera, however the onset of extension began following the end of thrusting associated with Sevier and Laramide contractional deformation (Sonder and Jones, 1999; Janecke, 2007). Several mechanisms have been proposed for the initiation of extension. A steepening of the subducting Farallon slab at ~53-51 Ma accompanied by a decreased rate of subduction led to detachment fault reactivation of fold and thrust belt aged deformation and the migration of magmatism westward in the direction of the backwards sinking slab (Constenius, 1996). Plate motion dynamics for the subducting slab changed to right-lateral shear relative to the North American plate, forming transtensional basins (Sonder and Jones, 1999; Miller et al., 2016). Delamination of the Farallon slab was occurring throughout this time from ~50-20 Ma, supported by the eruption of the voluminous mantle derived "ignimbrite flareup" throughout western North America (Armstrong and Ward, 1991; Humphreys, 1995). The actively evolving plate dynamics that led to this magmatism generated large-scale volcanic provinces in the foreland of the fold and thrust belt. The Absaroka

Volcanic Province extends from southeast Wyoming to southwest Montana with the bulk of magmatism occurring between ~55-44 Ma. Timing of Absaroka magmatism is coeval with the Challis Volcanic Province of east-central Idaho which was active from ~50-47 Ma (Chadwick, 1970; Feeley, 2003; Chetel et al., 2011). In addition to magmatism and the formation of extensional basins, Eocene extension facilitated the exhumation of metamorphic core complexes throughout the length of the Cordillera (e.g., the Anaconda and Bitterroot in southwest Montana, ~53-40 Ma; Coney and Harms, 1984; O'Neill et al., 2004; Schwartz et al., 2019).

Magmatism was prominent throughout the Miocene with the near synchronous eruption of the Columbia River Basalts and the inception of the Yellowstone hotspot (YSH). The voluminous Columbia River Basalts erupted in several pulses throughout the Pacific Northwest from ~17-15 Ma with the bulk of magmatism erupting over a relatively short span from ~16.6-15.9 Ma (Camp and Hanan, 2008, Kasbohm and Schoene, 2018). The onset of YSH magmatism overlapped temporally with the earliest of the Columbia River Basalt phases at ~17 Ma (Christiansen et al., 2002; Camp and Ross, 2004; Camp and Wells, 2021) although there are some that argue a more long-lived YSH model (e.g., Murphy et al., 1998; Eddy et al., 2017; Camp and Wells, 2021). The most accepted model for the YHS is that it is a deep-seated mantle plume interacting with a westward migrating overriding North American plate (Morgan, 1972; Anders and Sleep, 1992; Pierce and Morgan, 2009). The Eastern Snake River Plain (ESRP), which runs from approximately southwest Oregon to the hotspot's current location in northwest Wyoming, is an area of low topography and subsidence following the proposed track of hotspot migration (Fig. 1). Proposed mechanisms for low topography within the ESRP include (1) thermal contraction associated with cooling as the hotspot migrates eastward, and (2) crustal loading of dense mafic intrusions into and away from the plain, causing isostatic downwarping (Brott et al., 1981; McQuarrie and Rodgers, 1988; Anders and Sleep, 1992, Rodgers et al., 2002). As the YSH migrated eastward, the topographic swell created by the impingement of the hotspots plume source on the overriding ancestral North American crust has facilitated extension and active seismicity on each flank of the bow shaped region of high topography surrounding the hotspot

and ESRP referred to as the Yellowstone Crescent of High Terrain (YCHT) (Anders and Sleep, 1992; Rogers et al., 2002; Pierce and Morgan, 2009).

The approach and passage of the YSH from the early Miocene to present has been proposed to have facilitated uplift and subsidence within its path and the YCHT. Detrital zircon U-Pb provenance studies have been used to suggest that the bulge of the YSH beneath the crust produced a dynamic continental drainage divide forcing drainage to flow radially away from the location of the hotspot (Link et al., 2005; Beranek et al., 2006; Staisch et al., 2021). This dynamic drainage divide located over the active YHS center caused major reorganization of the paleo-Snake River (Beranek et al., 2006; Staisch et al., 2021). The reorganization of paleo drainage is also supported through the detailed stratigraphic analysis of northwest trending grabens throughout southwest Montana which record changes in source terranes coincident with changes in relief along the YCHT (Fritz and Sears, 1993; Sears et al., 2009). Differences between the location of the present-day drainage divide and the divide predicted from smoothed topography are suggested to be evidence of active drainage divide migration in the Yellowstone region (Wegmann et al., 2007). Increased exhumation along the northern flank of the YCHT contemporaneous with the passage of the YHS is shown in apatite (U-Th)/He data within the Pioneer Mountains of central Idaho, suggesting substantial landscape response to hotspot related processes (Vogl et al., 2014). The history of topographic change in this region is complex but the YSH has played a role in influencing landscape evolution and incision throughout its eastward migration.

Tectonics, Topography, and Magmatism in Southwest Montana

This study focuses on the northern Madison and Gallatin Ranges of southwest Montana on the northern flank of the YCHT (Fig. 1). Both ranges are underlain by metamorphosed Archean bedrock and overlain by Paleozoic and Mesozoic sedimentary sequences and Absaroka volcanic rocks in the Gallatin Range (Chadwick, 1969; Tysdal, 1986; Kellogg et al., 1995). The area was affected by Laramide compressional deformation and Cenozoic extension resulting in a complicated

and diverse tectonic history.

Timing of Laramide deformation has been difficult to constrain, fueling studies throughout western Montana. More recent work by Carrapa et al. (2019) and Garber et al. (2020) suggests the onset of deformation within Southwest Montana may have initiated earlier than ~81 Ma and potentially as early as 100 Ma. The Madison Range to the west of the Gallatin Range contains two major Laramide-age fault systems. The first is the northwest striking Spanish Peaks Reverse Fault that is part of the larger Bismark-Spanish Peaks-Gardiner Pre-Cambrian fault system which stretches from the western most part of the Tobacco Root Mountains across the Gallatin Range to the Montana-Wyoming border north of Yellowstone (Garihan et al., 1983; Tysdal et al., 1986; Kellogg et al., 1995). Although active during the Laramide, this fault has proposed middle Proterozoic ancestry and has been inactive since the Eocene as evidenced by undeformed cross cutting Absaroka Volcanics (Garihan et al., 1983; Kellogg et al., 1995). To the southwest of the Spanish Peaks Fault lies the near parallel north striking Hilgard Thrust and the Madison normal fault system that run nearly parallel to the Madison Range (Kellogg et al., 1995). The Hilgard Thrust system is cut by a Cretaceous (~68-69 Ma) dacite porphyry sill complex throughout sections of the Madison Range, particularly at the intrusive complex center within Lone Mountain (Tysdal et al., 1986; Kellogg et al., 1995; Kellogg et al., 2007). This cross-cutting relationship establishes the end of Laramide compression on this fault. The Madison Fault however has a continued history of activity from the Eocene to the Quaternary as evidenced by substantial displacement along the length of the fault and recurring intervals of seismicity (Haller et al., 2000; Haller et al., 2010).

Eocene extension brought widespread magmatism to regions across southwest Montana. The eruptions of the Absaroka Volcanic Province (AVP) contributed magma covering approximately 23,000 km² across southeast Wyoming to southwest Montana (Chadwick, 1969; Feeley, 2003; Chetel et al., 2011). The northern most range of the AVP extends as far as the Gallatin River to the west with continuous intrusion across the Gallatin Range from ~55-52 Ma (Chadwick, 1969; Feeley, 2003). Extensional magmatism was accompanied by synextensional sedimentation in basins throughout the

region (Fig. 1) including deposits of the post-compressional Renova Formation (Robinson and Barnett, 1963, Kuenzi and Fields, 1971; Hanneman and Wideman, 1991). This Eocene Formation is separated from the overlying Miocene Six Mile Creek Formation by an angular unconformity that lasted from ~20-16.5 Ma. The start of Six Mile Creek deposition after this hiatus in sedimentation was coeval with the eruption of the Columbia River Basalts, the inception of the YSH and northward propagation of Basin and Range extension (Constenius, 1996; Sears and Ryan, 2003).

The arrival of the YSH to its current location at the Yellowstone plateau occurred at ~2.05 Ma, contemporaneous with the eruption of the Huckleberry Ridge Tuff (Fritz and Sears, 1993; Pierce and Morgan, 2009). Continued progression of the hotspot persisted, generating seismicity and deformation within the YCHT as well as creating new northwest trending grabens that intersected with pre-existing Miocene grabens, with continued changes to drainage routes simultaneously affecting sedimentation (Pierce and Morgan, 2009; Sears et al., 2009; Staisch et al., 2021). Magmatism since the inception of the Yellowstone plateau has been intermittently active, erupting large volumes of material over an area $>6500 \text{ km}^3$, and contributing heat to hydrothermal features across the plateau (Christiansen, 1984).

(U-Th)/He Thermochronometry

The apatite (U-Th)/He (AHe) technique is a low temperature thermochronometer that takes advantage of the thermally activated diffusion within a mineral of ^4He , which is produced through the radioactive decay of U, Th and Sm. Diffusion and retentivity of ^4He is dependent on both internal crystal properties specific to individual mineral systems and temperature. Higher temperatures facilitate open system behavior with rapid diffusion of ^4He through the grain lattice to the grain boundary, while lower temperatures facilitate closed system behavior, causing retention of ^4He . The temperature range between the lower and upper limit of fully open and closed system behavior is the partial retention zone (PRZ) where there can be both retention and diffusion of ^4He . For the AHe, this temperature falls between ~40-90°C making it a low temperature thermochronometer and a useful

tool for inquiry involving processes within the upper ~1-4 km of the crust (Wolf et al., 1998; Farley, 2000; Ehlers and Farley, 2003; Flowers et al., 2009). The diffusion kinetics of apatite are affected by radiation damage to the crystal, with higher levels of radiation damage increasing the temperature sensitivity. Thus, correlations between dates and effective uranium (eU , $eU=[U]+0.234*[Th]+0.0046*[Sm]$, a proxy for radiation damage) are sometimes expected depending on a sample's thermal history (Shuster et al., 2006; Flowers et al., 2009; Gautheron et al., 2009). Additional factors that can cause variability of grain dates include grain shape and size (Reiners and Farley, 2001; Cooperdock et al., 2019), the presence of inclusions that act as either He traps and/or contribute excess He from foreign minerals (Vermeesch et al., 2007), He implantation from surrounding U-Th rich sources (Spiegel et al., 2009), grains that are broken or fractured leading to additional diffusion of He out of the system (Brown et al., 2013), and zonation of parent nuclides within the grain (Farley et al., 2011). Helium is emitted energetically, so an alpha-ejection correction (F_T) is applied based on grain size and shape to account for He ejected from the crystal (Wolf et al., 1996; Ketcham et al., 2011).

Methods

Strategy and Samples

Our sampling strategy targeted Tertiary-Cretaceous igneous intrusions. The lithologies of those samples include Cretaceous dacite and dacite porphyry, Tertiary Cretaceous felsic intrusions, Tertiary-Cretaceous gabbro, and two non-mapped dikes. Many of these are a part of the larger Fan and Lone Mountain intrusive center made up of dacite porphyry sills and sometimes referred to as a Christmas-tree Laccolith complex (Kellogg & Harlan, 2007; Vuke, 2013). These lithologies are likely to contain apatite and zircon, and their proposed age post-dates Laramide deformation, increasing the probability that any measurable exhumation is caused by more recent, lower magnitude tectonic processes. Additionally, these younger intrusions may exhibit less radiation damage than would have affected surrounding older rocks. Based on this, these samples were selected as promising candidates

to reconstruct the post-Laramide exhumation history of this region using the apatite (U-Th)/He (AHe) system.

Bedrock samples were collected as three separate transects within the northern Madison and Gallatin Ranges. Two transects were collected over as large an elevation range as possible within the Gallatin River Valley (the Big Sky and Gallatin Gateway transects, Fig. 2). A third transect was collected just west of the Big Sky transect approaching the Madison Fault (the Madison Range transect, Fig. 2). This study is attempting to determine if there is any Yellowstone hotspot driven exhumation and how far that signal may reach. This study area is ideal for investigating this question because of its proximity to the hotspot and lack of active quaternary faults besides the Madison Fault to the west along the northern Madison Range (Kellogg and Williams, 1998; Vuke, 2013). The Madison Range transect is unique from the other two transects because these samples were collected as a horizontal transect with little difference in elevation in order to determine if there is any difference in exhumation with proximity to the Madison Fault (Haller et al., 2000; Haller et al., 2010). Additionally, this region is far enough from the region of Quaternary glaciation in the Yellowstone region, which should limit any influence from glacial erosion and allow us to measure exhumation from other tectonic processes (Pierce et al., 2014). Each transect contains 6-7 samples for a total of 18 samples. We analyzed 5-8 individual apatite grains per sample, contributing to an average AHe date for that sample. The Big Sky transect has the largest relief of 1440 m from the highest to lowest elevation sample, followed by the Madison Range with sample elevations spanning 481 m, and lastly the Gallatin Gateway with samples collected over 355 m. For the elevation transects, bedrock samples were collected ~200 vertical m apart to produce a pseudo-vertical profile of the crust using the natural topographic relief of the region. This sampling strategy is useful for observing differences in exhumation rate between lower and higher elevations within the same transect and establishing age-elevation relationships (AER; Braun, 2002).

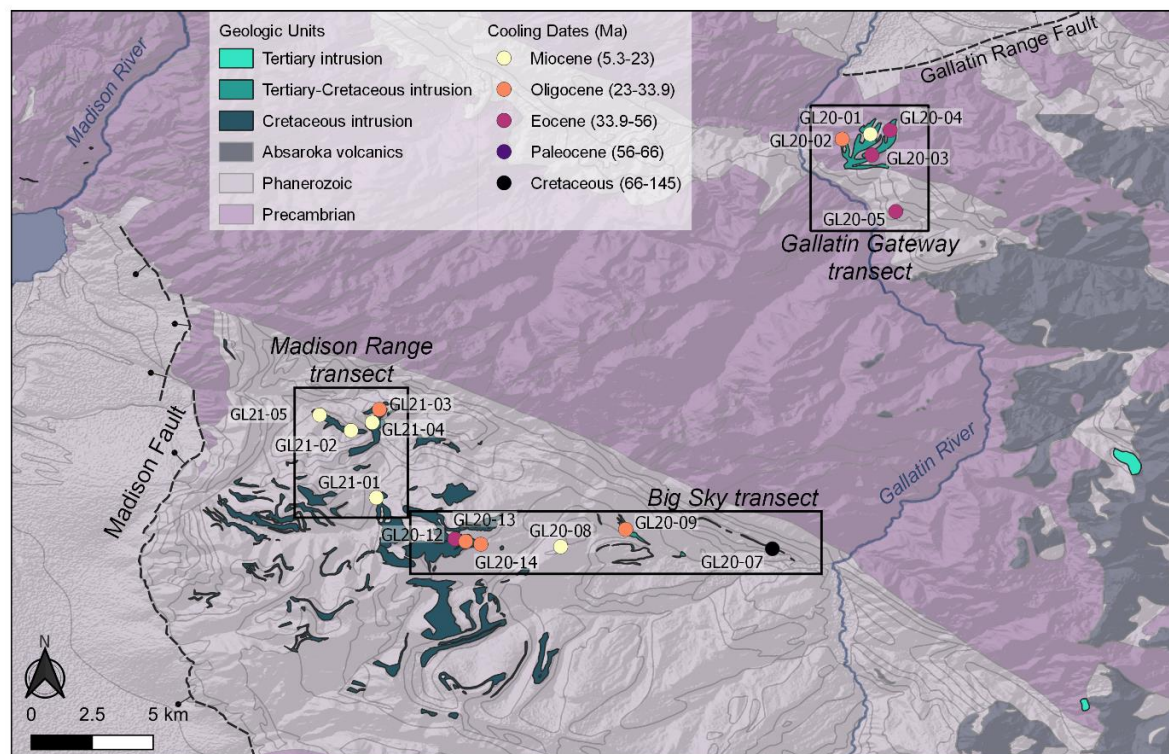


Fig. 2: Simplified geologic map of our study area (outlined in the white box of Fig. 1) with sample localities shown as circles colored by their average AHe date. Map shows sample locations in the Gallatin Gateway transect in the Gallatin Range and the Big Sky and Madison Range transects in the Madison Range outlined in black boxes with targeted intrusions highlighted. Other features of interest include the Madison Fault and eastern extent of Absaroka Volcanics east of the Gallatin River Valley.

Apatite (U-Th)/He Methods

Standard mineral separation techniques using density and magnetic separation were used to isolate apatite and zircon crystals in each sample. Two samples did not yield useable apatite grains, bringing the total to 16 samples analyzed. Individual apatite crystals were selected for AHe analyses by hand using a Leica M165C Stereoscope based on grain size, shape, and lack of inclusions. Acceptable grain sizes were those with a b-axis measurement larger than the standard baseline grain size of $\sim 60 \mu\text{m}$ (Farley et al., 1996; Wolf et al., 1996). Larger grains together with variables such as parent isotope concentration, grain geometry, and ejected ^4He stopping distances specific to each mineral system, contribute to a desired calculated alpha-ejection correction (F_T) value $> \sim 0.58$ (Wolf et al., 1996; Flowers et al., 2009; Ketcham et al., 2011). Measurements and images of each selected apatite grain were recorded prior to packing into Nb tube packets for analysis. Grains were analyzed for U, Th, Sm, and He concentrations at the University of Colorado (CU) Thermochronology

Research and Instrumentation Laboratory (CU TRaIL), Boulder, Colorado, USA. Grain packets were loaded into an ASI Alphachron™ for He extraction and measurement. Degassed grains were dissolved and spiked and then analyzed for U, Th, and Sm content using an Agilent 7900 Quadrupole inductively coupled plasma-mass spectrometer (ICP-MS). Concentrations of U, Th, and Sm were used to calculate He dates and all associated data with a custom spreadsheet using the methods described in Ketcham et al. (2011) and Cooperdock et al. (2019).

Thermal History Modeling Methods

To investigate the range of possible thermal histories compatible with our AHe data, we used the inverse modeling capabilities of the thermal history modeling software HeFTy (v.1.9.3; Ketcham, 2005) to evaluate time-temperature (t-T) paths and explore cooling histories for each transect. HeFTy uses a Monte Carlo approach to produce t-T paths that satisfy any geologic constraints set by the user and compares the predicted thermochronometric date with the observed data. HeFTy saves statistically defined paths which produce good or acceptable fits (Ketcham, 2005) which are used for interpretation. The details of the constraints used in this study are described in Table 2. Each sampled unit is mapped as either Cretaceous, Tertiary-Cretaceous, or Tertiary (Vuke et al., 2002; Kellogg and Williams, 2006), but only one radiometric age is available for these intrusions. We used an $^{40}\text{Ar}/^{39}\text{Ar}$ emplacement age of 69 ± 1 Ma for all samples which was acquired for a Cretaceous dacite porphyry in the Madison Range by Tysdal et al. (1986). Cretaceous intrusions within the Madison Range and Big Sky regions have been described as part of the same intrusive sill complex (Garihan et al, 1983; Tysdal et al., 1986; Kellogg and Harlan, 2007) and other rocks sampled are mostly lithologically similar, so using this date as the age of emplacement for all our samples is a reasonable assumption. The temperature range used was $>120^\circ\text{C}$ at the time of emplacement, the upper limit of AHe temperature sensitivity and radiation damage accumulation (Flowers et al., 2009). A second constraint was added to the model that allowed for reheating up to 350°C from ~ 55 to 52 Ma (Table 2). This additional geologic constraint represents a possible Absaroka related reheating event that is spatially

plausible for each sample and suggested based on interpretations of $^{40}\text{Ar}/^{39}\text{Ar}$ biotite and hornblende ages from other locations in the intrusive complex (Kellogg and Harlan, 2007). Differences between biotite and hornblende $^{40}\text{Ar}/^{39}\text{Ar}$ ages support a scenario with a possible reheating episode to temperatures of $\sim 300\text{-}500^\circ\text{C}$, which may have “reset” the biotite without affecting the hornblende due to the differences in their respective closure temperatures (Kellogg and Harlan, 2007). This region lacks any observed metamorphosed shales which would require temperatures in excess of $\sim 350^\circ\text{C}$ to form, therefore reducing the upper boundary of the possible reheating episode to $\sim 350^\circ\text{C}$ (Fig. 1; Kellogg and Harlan, 2007). Finally, each sample has surface temperature constraint of 5.9°C consistent with current average surface temperatures in the region (Gunderson, 2011).

Sample data input into HeFTy consisted of average values for grains for each sample separated into two bins based on eU (Table 2). The parameters of these bins are consistent across all samples and are defined as $\text{eU} < 20$ ppm or $\text{eU} > 20$ ppm. Two samples had high eU values and young dates; these samples were modeled as 1 bin due to difficulties finding good and acceptable paths with 2 bins (Table 2). Bin averages are entered into HeFTy as “synthetic grains” for each sample with average values for each grain bin for estimated spherical radius (ESR), uncorrected date, and concentrations of U, Th, and Sm. Uncertainty for each grain is the standard deviation of each bin or 10% of the bin mean, whichever is larger. The parameter used for He kinetics is the radiation damage accumulation and annealing model (RDAAM) as defined in Flowers et al. (2009) and the α -ejection correction (F_T) from Ketchum et al. (2011). Models for each sample were run until HeFTy produced 500 good fit paths.

TABLE 2: THERMAL HISTORY MODEL INPUTS FOR SOUTHWEST MONTANA SAMPLES

1. Thermochronologic data			
Samples and data used in simulations			
Sample	Rock type	eU bins for AHe data ^a	Emplacement age used in model
<u>Gallatin Gateway</u>			
GL20-01	TKfi (Tertiary-Cretaceous felsic intrusion)	<20 ppm (3 grain), >20 ppm (2 grains)	69 ± 1 Ma (Tysdal et al., 1986)
GL20-02	TKfi	<20 ppm (4 grains), >20 ppm (1 grain)	
GL20-03	TKfi	<20 ppm (4 grains), >20 ppm (1 grain)	
GL20-04	TKfi	<20 ppm (4 grains), >20 ppm (2 grain)	
GL20-05	Tia (Tertiary Absaroka intrusion)	<20 ppm (4 grains)	
<u>Big Sky</u>			
GL20-07	Gabbro dike	<20 ppm (3 grains)	
GL20-09	TKga (Tertiary-Cretaceous gabbro)	<20 ppm (1 grains), >20 ppm (3 grain)	
GL20-12	Kdap (Cretaceous dacite porphyry)	4 grains averaged, no bin	
GL20-13	Kdap	<20 ppm (4 grains)	
GL20-14	Kdap	<20 ppm (4 grains)	
<u>Madison Range</u>			
GL21-01	Kdap	<20 ppm (4 grains)	
GL21-02	Kdap	5 grains averaged, no bin	
GL21-03	Kdap	<20 ppm (4 grains)	
GL21-05	Kdap	<20 ppm (4 grains)	
<u>AHe data treatment: Ages, uncertainties, and other relevant constraints</u>			
Treatment: Samples were binned into groups with similar eU values, and the mean of each group was modeled			
He dates (Ma): Mean uncorrected He date of each bin. a-ejection corrected in HeFTy using Ketcham et al (2011).			
^a Ejection correction in HeFTy using Ketcham et al. (2011).			
Error (Ma) applied in modeling: The 1 σ sample standard deviation of each bin was applied if $\geq 10\%$. If $< 10\%$, then 10% was applied.			
r (um): Mean equivalent spherical radius of each bin			
eU (ppm): Mean U and Th for each bin			
eU zonation: none assumed			
<u>2. Additional geologic information</u>			
Constraint	Explanation and data source		
<u>All rocks (Gabbro dike, Kdap, TKfi, Tkga, Tia)</u>			
(1)	>120°C at time of emplacement	Dactite porphyry intrusions emplaced.	
(2)	300-350° at 55-52 Ma	Temperature range allows for but does not require an early Tertiary reheating episode related to possible reach of Absaroka Volcanics (Chadwick, 1969; Feeley, 2003; Kellogg et al., 2007).	
(3)	5.9°C at present day		
<u>3. System and model specific parameters</u>			
He kinetic model: RDAAM (radiation damage accumulation and annealing model; Flowers et al., 2009).			
Statistical fitting criteria: GOF values >0.5 for "good" fits. >0.05 for "acceptable" fits. The good-fits also must have a minimum GOF of 1/(N+1) where N is number of statistics used (Ketcham et al., 2005).			
Modeling Code: AHe uses HeFTy v1.9.3.			
Number of t-T paths attempted: 500 good-fit paths for all models.			

Results

Individual apatite grains from 16 samples were analyzed (5-8 grains per sample) totaling 84 grains. All data is reported in Table 1. Individual AHe dates and 2σ analytical uncertainties are reported for each grain alongside average dates for each sample with associated 1σ standard deviation. A total of 5 grains were rejected as outliers as determined by the Grubb's statistical test for outliers (Grubbs, 1969) and are reported in italics but omitted from date averages and final interpretations. Five additional grains were omitted from reporting and interpretation due to α -ejection correction (F_T) values <0.58 , which are considered unreliable. Sample ages that result in a coefficient of variation >0.2 (sample standard deviation/sample average, $>20\%$ dispersion) are considered dispersed and the sample average is not considered representative. Fourteen samples resulted in 18% or less dispersion with reported mean dates between 70 ± 3.4 Ma and 6.4 ± 0.28 Ma (Table 1). Two samples resulted in dispersion $>20\%$ (GL20-08, 57% dispersion; GL21-04, 29% dispersion). Since dates within these samples are not correlated with factors that are known to affect diffusion behavior (i.e., eU, grain size) we do not feel that the average dates for these samples are representative, and they have been omitted from inverse modeling and interpretations.

The Gallatin Gateway transect is the northernmost transect and covered 355 m of elevation with a wide range of AHe cooling dates from 43.0 ± 4.3 Ma to 14.5 ± 2.2 Ma (Fig. 2, Fig. 3). This Gallatin Transect is the furthest of all three transects from the YSH and has older average date values for similar elevations compared to the other transects. Samples from both the highest and lowest elevations have similar average date values, and there is no observable spatial trend related to date and elevation among samples within this transect (Fig. 6). Plots for eU versus average AHe dates for this transect show a range of dates across similar eU values and lacks any sort of general trend (Fig. 3).

The Big Sky transect has the largest elevation range of the three transects with 1440 m separating the highest and lowest samples (Fig. 2, Fig. 4). AHe cooling dates for this transect span a

wide range from 70.5 ± 3.4 Ma to 23.9 ± 3.3 Ma. The larger elevation difference between the highest and lowest samples results in a vertical profile with a larger age spread between samples. This transect shows a more expected positive trend among date-elevation values (Fig. 6) with older dates at higher elevations and younger dates and lower elevations. The oldest AHe date within this transect (70.5 ± 3.4 Ma, GL20-07) does not follow this trend as it has the lowest elevation and oldest average date. This date may likely reflect the age of emplacement for this sample because it overlaps with a previously established $^{40}\text{Ar}/^{39}\text{Ar}$ emplacement age for this intrusion (69 ± 1 Ma, Tysdal, 1986). Although we can establish a positive slope trend between date and elevation, similar dates are observed across a range of eU values showing there is no observable trend between eU and AHe date for this transect (Fig. 4).

Average sample dates from the Madison Range transect have the youngest dates of all three transects ranging from 26.9 ± 4.9 Ma to 6.5 ± 0.28 Ma over 481 m of relief (Fig. 2, Fig. 5). The clustered nature of this transect is intentional and was collected in this manner to quantify any relationship between cooling and proximity to the Madison Fault. Although there is no observable trend between average sample age and elevation (Fig. 6) or eU (Fig. 5), there may be a relationship between AHe date and fault distance. Figure 7 shows three samples within the Madison Range transect that are increasing in date with increased distance from the fault. One sample (6.5 ± 0.28 Ma, GL21-01) has an anomalously young date for its high elevation that does not fit within this trend.

The Madison Range and Big Sky transects are spatially close to one another and could be considered together. Samples in this combined transect show both an increase in AHe age with elevation (Fig. 6) and an increase in AHe age with distance from the Madison Fault (Fig. 7), though the wide range in elevation for the Big Sky transect makes this relationship more complex to interpret.

TABLE 1: APATITE (U-Th)/He DATA FROM SOUTHWEST MONTANA

Sample ^a	Mass (μ g)	r (mm) ^b	Termination ^c	⁴ He (nmol/g)	U (ppm)	Th (ppm)	Sm (ppm)	eU ^d	Th/U	Raw Age (Ma)	F _T ^e	Corrected Age (Ma) ^f	2s ^f (Ma)
Gallatin Gateway transect													
GL20-01: Tertiary-Cretaceous felsic intrusion (TKfi): 45.4897°N, -111.2325°W, 2189 m elevation													
a1	3.68	56.8	1T	0.62	7.51	23.45	106.4	13.22	3.12	8.67	0.74	11.74	0.54
a2	2.84	56.5	2T	1.44	10.61	50.87	295.7	23.07	4.79	11.57	0.73	15.74	0.60
a3	6.52	68.6	2T	1.36	10.69	29.89	129.9	17.96	2.80	14.08	0.78	17.96	0.71
a4	5.52	66.6	1T	0.82	7.65	28.88	128.6	14.68	3.77	10.40	0.77	13.41	0.76
a5	1.62	47.3	2T	1.11	10.65	46.79	207.8	22.04	4.39	9.34	0.68	13.62	0.88
Mean: 14.49±0.70 Ma, 15% dispersion													
GL20-02: Tertiary-Cretaceous felsic intrusion (TKfi): 45.4871°N, -111.2472°W, 2006 m elevation													
a1	1.16	36.3	2T	0.66	6.55	5.64	151.8	8.07	0.86	15.24	0.61	24.66	2.85
a2	2.96	55.0	2T	1.01	7.03	11.52	135.3	9.94	1.64	18.88	0.73	25.58	2.50
a3	2.48	52.3	2T	2.22	18.42	6.70	186.6	20.24	0.36	20.30	0.73	27.76	1.68
a4	1.00	37.9	2T	0.61	3.83	5.30	106.8	5.22	1.39	21.75	0.62	34.55	5.56
a5	4.03	59.1	1T	0.70	3.99	7.08	110.1	5.81	1.77	22.29	0.75	29.48	1.81
Mean: 28.41±2.88 Ma, 12% dispersion													
GL20-03: Tertiary-Cretaceous felsic intrusion (TKfi): 45.4788°N, -1114.2317°W, 2120 m elevation													
a1	0.76	34.3	2T	0.57	4.94	5.23	113.6	6.33	1.06	16.71	0.59	28.06	5.12
a2	4.06	62.1	2T	0.97	4.10	5.92	105.8	5.63	1.45	31.98	0.76	41.58	2.15
a3	5.82	69.6	2T	7.08	42.84	0.68	39.9	43.05	0.02	30.45	0.80	38.15	1.94
a4	2.02	50.3	2T	1.32	8.77	6.91	166.2	10.62	0.79	23.05	0.72	32.04	3.08
a5	2.97	56.7	2T	1.67	6.50	14.91	127.0	10.20	2.30	30.32	0.74	40.83	1.91
Mean: 36.13±2.84 Ma, 15% dispersion													
GL20-04: Tertiary-Cretaceous felsic intrusion (TKfi): 45.4917°N, -111.2221°W, 2339 m elevation													
a1	4.09	63.86	2T	29.93	133.47	62.95	57.2	148.52	0.47	37.31	0.78	48.01	1.04
a5	1.25	42.71	2T	1.24	4.40	25.91	221.3	10.83	5.89	21.18	0.65	32.39	4.70
a6	1.43	44.36	2T	2.20	6.01	32.56	201.9	14.00	5.42	29.10	0.66	43.74	2.72
a7	1.16	42.53	2T	3.92	22.98	15.45	244.3	26.95	0.67	26.93	0.67	40.21	4.50
a8	1.05	40.86	2T	2.18	8.81	26.78	226.2	15.46	3.04	26.19	0.64	40.59	2.34
a9	0.96	39.12	2T	0.95	3.75	10.64	171.0	6.48	2.84	27.10	0.63	42.68	3.34
Mean: 41.27±3.11 Ma, 13% dispersion													
GL20-05: Tertiary intrusion Absaroka (Tia): 45.4492°N, -111.2193°W, 1984 m elevation													
a6	0.63	31.75	1T	1.78	11.14	25.48	156.3	17.39	2.29	19.03	0.55	34.41	2.40
a7	1.63	42.32	1T	1.81	7.89	22.49	126.0	13.40	2.85	25.08	0.65	38.24	1.53
a8	1.96	47.93	1T	2.97	11.28	37.91	95.1	20.41	3.36	26.99	0.69	39.03	1.92
a9	0.91	35.61	2T	2.53	8.87	31.81	129.3	16.59	3.59	28.26	0.59	47.75	2.19
a10	2.81	51.75	1T	2.02	5.80	22.32	96.5	11.23	3.85	33.39	0.71	46.82	2.87
Mean: 42.96±2.13 Ma, 10% dispersion													

Note: Rows in italics indicate grains that are outliers from the main population and not included in averages.

^aMean and 1 σ standard deviation of corrected dates reported for samples with <20% dispersion. No mean reported for samples with >20% dispersion. Dispersion is the standard deviation divided by the mean of the sample.

^bEquivalent spherical radius (r), the radius of a sphere with the same surface area to volume ratio.

^cType of grain terminations: 2T—whole grain; 1T—one tip broken off; 0T—both tips broken off.

^deU: Effective uranium concentration, weights U and Th for their alpha productivity, compiled as [U] + 0.235 * [Th].

^eF_T is alpha-ejection correction of Ketcham et al. (2011).

^fAnalytical uncertainty based on U, Th, He, and grain-length measurements.

TABLE 1: APATITE (U-Th)/He DATA FROM SOUTHWEST MONTANA (continued)

Sample ^a	Mass (μ g)	r (mm) ^b	Termination ^c	⁴ He (nmol/g)	U (ppm)	Th (ppm)	Sm (ppm)	eU ^d	Th/U	Raw Age (Ma)	F _T ^e	Corrected Age (Ma) ^f	2s ^f (Ma)
Big Sky transect													
GL20-07: Unmapped gabbro dike: 45.2728°N, -111.2837°W, 1950 m elevation													
a6	0.75	35.1	2T	1.24	2.69	12.03	105.9	5.68	4.47	40.32	0.58	68.64	6.94
a7	1.25	41.9	2T	1.48	2.68	11.67	97.44	5.58	4.35	49.03	0.64	75.32	6.78
a8	0.78	34.5	1T	0.99	3.20	10.00	90.73	5.69	3.13	32.26	0.58	55.22	6.51
a9	1.02	37.6	1T	1.96	1.93	9.20	77.79	4.21	4.77	86.17	0.61	140.5	11.85
a10	1.37	43.3	1T	0.99	1.88	9.08	71.34	4.12	4.84	44.66	0.65	67.65	10.05
Mean: 70.54 ± 7.92 Ma, 5% dispersion													
GL20-08: Cretaceous dacite porphyry intrusion (Kdap): 45.2739°N, -111.3943°W, 2650 m elevation													
a1	1.06	38.6	2T	0.31	5.11	11.37	114.8	7.96	2.22	7.16	0.62	11.39	1.70
a2	1.48	38.2	1T	0.17	3.38	11.42	104.4	6.22	3.38	5.00	0.62	8.04	1.69
a3	1.55	35.6	0T	0.25	3.18	10.99	123.3	5.95	3.45	7.66	0.59	12.83	1.47
a4	1.59	45.3	2T	0.65	4.13	14.42	146.7	7.73	3.50	15.54	0.67	22.95	2.65
a5	1.36	38.7	1T	0.43	4.69	13.80	130.5	8.13	2.95	9.72	0.62	15.49	1.91
a6	2.65	51.0	0T	0.78	2.48	10.56	100.1	5.11	4.27	28.37	0.71	39.90	2.50
a7	1.72	44.1	0T	0.22	4.02	14.35	131.8	7.60	3.56	5.34	0.66	7.99	0.67
a8	2.20	45.8	0T	0.55	2.99	9.69	105.0	5.42	3.25	18.85	0.68	27.63	1.76
57% dispersion of AHe dates													
GL20-09: Tertiary-Cretaceous gabbro (TKga): 45.2830°N, -111.3603°W, 2204 m elevation													
a1	2.30	41.31	0T	1.00	7.50	30.64	200.7	15.0	4.09	12.36	0.64	19.18	1.42
a2	1.03	36.66	1T	1.90	9.84	51.80	281.6	22.5	5.27	15.70	0.59	26.21	2.38
a3	2.06	38.46	1T	3.88	19.11	96.26	291.7	42.4	5.04	17.02	0.61	27.66	1.80
a4	0.87	31.16	1T	0.73	7.22	38.53	264.0	16.7	5.34	8.14	0.53	15.20	2.16
a5	4.57	52.81	1T	2.12	9.25	64.26	168.6	24.7	6.94	15.94	0.71	22.38	1.13
Mean: 23.86 ± 1.68 Ma, 14% dispersion													
GL20-12: Cretaceous dacite intrusion (Kda): 45.2779°N, -111.4495°W, 3390 m elevation													
a1	7.58	71.31	1T	5.06	22.24	25.94	95.59	28.53	1.17	32.86	0.80	41.24	1.80
a2	1.33	39.32	2T	6.03	36.98	4.61	116.88	38.22	0.12	29.24	0.65	45.12	4.07
a3	0.96	39.33	2T	5.85	27.17	38.06	210.00	36.48	1.40	29.73	0.64	46.61	2.80
a4	1.96	41.66	2T	1.92	5.91	19.00	128.81	10.59	3.21	33.70	0.65	51.82	2.07
a5	0.73	31.09	2T	1.13	4.75	15.27	115.00	8.52	3.22	24.53	0.54	45.28	5.60
Mean: 46.20 ± 2.68 Ma, 8% dispersion													
GL20-13: Cretaceous dacite (Kda): 45.2767°N, -111.4439°W, 3109 m elevation													
a1	0.73	32.57	2T	0.78	3.73	17.60	133.6	8.08	4.71	17.88	0.549	32.16	10.771
a2	2.47	54.02	2T	2.01	12.79	20.31	155.9	17.81	1.59	20.91	0.73	28.55	1.7879
a3	1.48	42.87	2T	0.73	4.09	18.35	118.9	8.60	4.49	15.66	0.652	23.88	3.6926
a4	0.95	35.76	2T	0.89	3.89	17.00	142.6	8.11	4.37	20.29	0.587	34.15	8.1346
a5	0.90	35.30	2T	0.68	3.27	12.82	116.9	6.46	3.92	19.43	0.584	32.88	10.387
Mean: 29.87 ± 6.8 Ma, 14% dispersion													
GL20-14: Cretaceous dacite porphyry (Kdap): 45.2752°N, -111.4359°W, 2948 m elevation													
a1	2.47	51.09	2T	2.25	9.07	27.15	159.0	15.73	2.99	26.51	0.709	37.22	3.08
a2	3.81	58.19	2T	2.17	10.93	18.74	116.5	15.53	1.71	25.89	0.748	34.51	1.99
a3	10.1	78.08	2T	1.72	8.27	23.14	89.98	13.88	2.80	23.05	0.808	28.46	1.31
a4	2.23	50.36	2T	1.57	8.32	26.65	156.2	14.85	3.20	19.58	0.705	27.68	2.26
a5	3.01	55.26	2T	3.90	6.98	23.02	133.6	12.62	3.30	57.16	0.73	77.96	4.81
Mean: 31.97 ± 2.16 Ma, 13% dispersion													

Note: Rows in italics indicate grains that are outliers from the main population and not included in averages.

^aMean and 1 σ standard deviation of corrected dates reported for samples with <20% dispersion. No mean reported for samples with >20% dispersion. Dispersion is the standard deviation divided by the mean of the sample.

^bEquivalent spherical radius (r), the radius of a sphere with the same surface area to volume ratio.

^cType of grain terminations: 2T—whole grain; 1T—one tip broken off; 0T—both tips broken off.

^deU: Effective uranium concentration, weights U and Th for their alpha productivity, compiled as [U] + 0.235 * [Th].

^eF_T: is alpha-ejection correction of Ketcham et al. (2011).

^fAnalytical uncertainty based on U, Th, He, and grain-length measurements.

TABLE 1: APATITE (U-Th)/He DATA FROM SOUTHWEST MONTANA (continued)

Sample ^a	Mass (µg)	r (mm) ^b	Termination ^c	⁴ He (nmol/g)	U (ppm)	Th (ppm)	Sm (ppm)	eU ^d	Th/U	Raw Age (Ma)	F _T ^e	Corrected Age (Ma) ^f	2s ^g (Ma)
Madison Range transect													
GL21-01: Cretaceous dacite porphyry (Kdap): 45.2996°N, -111.4906°W, 2165m elevation													
a1	1.5	41.7	2T	0.29	11.3	21	179.7	16.5	1.865	3.2	0.65	4.9	0.4
a2	1.7	46.9	2T	0.31	6.6	23.9	150.6	12.5	3.597	4.7	0.68	6.8	0.5
a3	4.8	62.6	2T	0.28	5.4	23.7	105	11.2	4.368	4.7	0.76	6.1	0.4
a4	1.3	43.2	2T	0.39	7.9	34.6	196.2	16.4	4.354	4.4	0.65	6.7	0.5
a5	5.1	68.3	2T	0.24	4.9	16.5	111.7	9	3.363	4.9	0.78	6.3	0.3
Mean: 6.48±0.42 Ma, 4% dispersion													
GL21-02: Cretaceous dacite porphyry (Kdap): 45.3347°N, -111.5038°W, 1901m elevation													
a1	1.64	44.1		1.64	8.47	35.52	203.0	17.17	4.19	17.76	0.66	26.71	1.92
a2	2.49	54.4		1.71	10.03	34.00	178.1	18.34	3.39	17.28	0.73	23.74	1.61
a3	2.51	53.2		1.66	10.30	33.51	173.2	18.48	3.25	16.68	0.72	23.10	1.12
a4	4.58	66.3		2.35	13.64	55.03	172.6	26.95	4.03	16.18	0.77	20.91	1.11
a5	1.66	46.7		1.81	15.19	61.06	244.0	30.01	4.02	11.21	0.68	16.43	0.95
Mean: 22.18±1.3 Ma, 15% dispersion													
GL21-03: Cretaceous dacite porphyry (Kdap): 45.3458°N, -111.4890°W, 2322m elevation													
a1	6.21	73.0	2T	1.11	4.75	19.68	94.33	9.55	4.14	21.47	0.79	27.03	1.09
a2	3.61	54.3	2T	0.85	4.55	16.26	95.23	8.54	3.57	18.51	0.72	25.45	1.99
a3	5.67	71.4	2T	4.00	13.74	16.54	184.4	17.90	1.20	41.31	0.80	51.76	3.33
a4	2.67	51.7	2T	0.88	5.69	21.79	130.1	11.03	3.83	14.78	0.71	20.72	1.35
a5	1.87	44.4	2T	1.67	6.94	27.13	152.3	13.58	3.91	22.87	0.66	34.23	3.25
Mean: 26.86±1.92 Ma, 18% dispersion													
GL21-04: Cretaceous dacite porphyry (Kdap): 45.3389°N, -111.4926°W, 2222m elevation													
a1	8.62	81.34	2T	0.61	9.35	10.61	87.15	11.97	1.13	9.40	0.82	11.43	0.51
a2	4.99	60.15	1T	0.76	4.77	22.20	101.2	10.17	4.65	13.81	0.75	18.39	1.39
a3	9.43	79.92	2T	0.74	5.28	23.97	86.47	11.08	4.54	12.43	0.81	15.32	0.62
a4	8.19	76.95	2T	1.27	5.47	24.86	97.34	11.50	4.55	20.50	0.80	25.50	0.77
a5	4.91	64.92	2T	0.67	5.60	24.80	118.5	11.64	4.43	10.66	0.77	13.87	0.73
29% dispersion of AHe dates													
GL21-05: Cretaceous dacite porphyry (Kdap): 45.3429°N, -111.5202°W, 1841m elevation													
a1	1.50	42.34	2T	2.76	35.68	13.23	229.4	39.10	0.37	13.11	0.67	19.57	1.01
a2	3.66	60.64	2T	0.50	8.04	28.73	160.8	15.07	3.58	6.14	0.75	8.13	0.65
a3	6.19	71.39	2T	0.46	6.44	23.67	117.2	12.22	3.68	7.01	0.79	8.86	0.50
a4	4.13	59.72	2T	0.46	5.99	24.21	133.8	11.91	4.04	7.18	0.75	9.57	0.43
a5	4.63	65.12	2T	0.59	10.82	24.60	131.1	16.83	2.27	6.46	0.77	8.35	0.39
Mean: 8.73±0.49 Ma, 6% dispersion													

Note: Rows in italics indicate grains that are outliers from the main population and not included in averages.

^aMean and 1σ standard deviation of corrected dates reported for samples with <20% dispersion. No mean reported for samples with >20% dispersion. Dispersion is the standard deviation divided by the mean of the sample.

^bEquivalent spherical radius (r), the radius of a sphere with the same surface area to volume ratio.

^cType of grain terminations: 2T—whole grain; 1T—one tip broken off; 0T—both tips broken off.

^deU: Effective uranium concentration, weights U and Th for their alpha productivity, compiled as [U] + 0.235 * [Th].

^eF_T is alpha-ejection correction of Ketchum et al. (2011).

^fAnalytical uncertainty based on U, Th, He, and grain-length measurements.

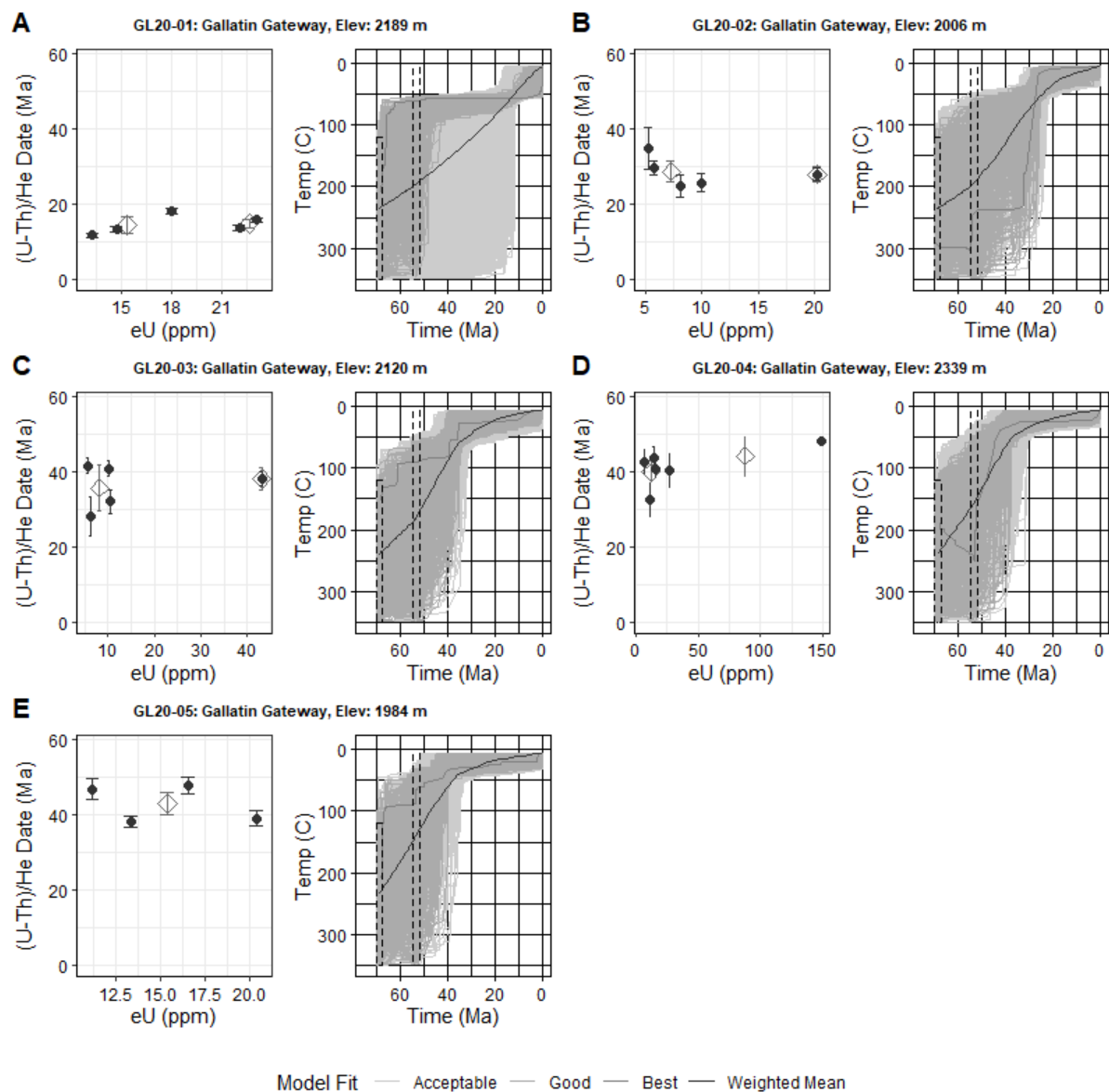


Fig. 3: (A-E) AHe eU and thermal modeling results for all samples in the Gallatin Gateway transect with $<20\%$ dispersion (standard deviation divided by the sample mean). Date eU plots have outlier grains plotted in light grey but not modeled or used in interpretations. Error bars for sample points are the 2σ analytical uncertainties of individual corrected grain dates and may be obscured by points. Sample averages in each bin are plotted as open diamonds with error bars equal to the standard deviation or 10% of the mean date, whichever is greater. Thermal history plots show modeling constraints as dashed boxes, the weighted mean (black line), best fit path (dark grey), good fit paths (gray) and acceptable fit paths (light grey). Thermal history modeling constraints for all modeled samples are listed in Table 2. Abbreviations: Elev – elevation, Temp – temperature.

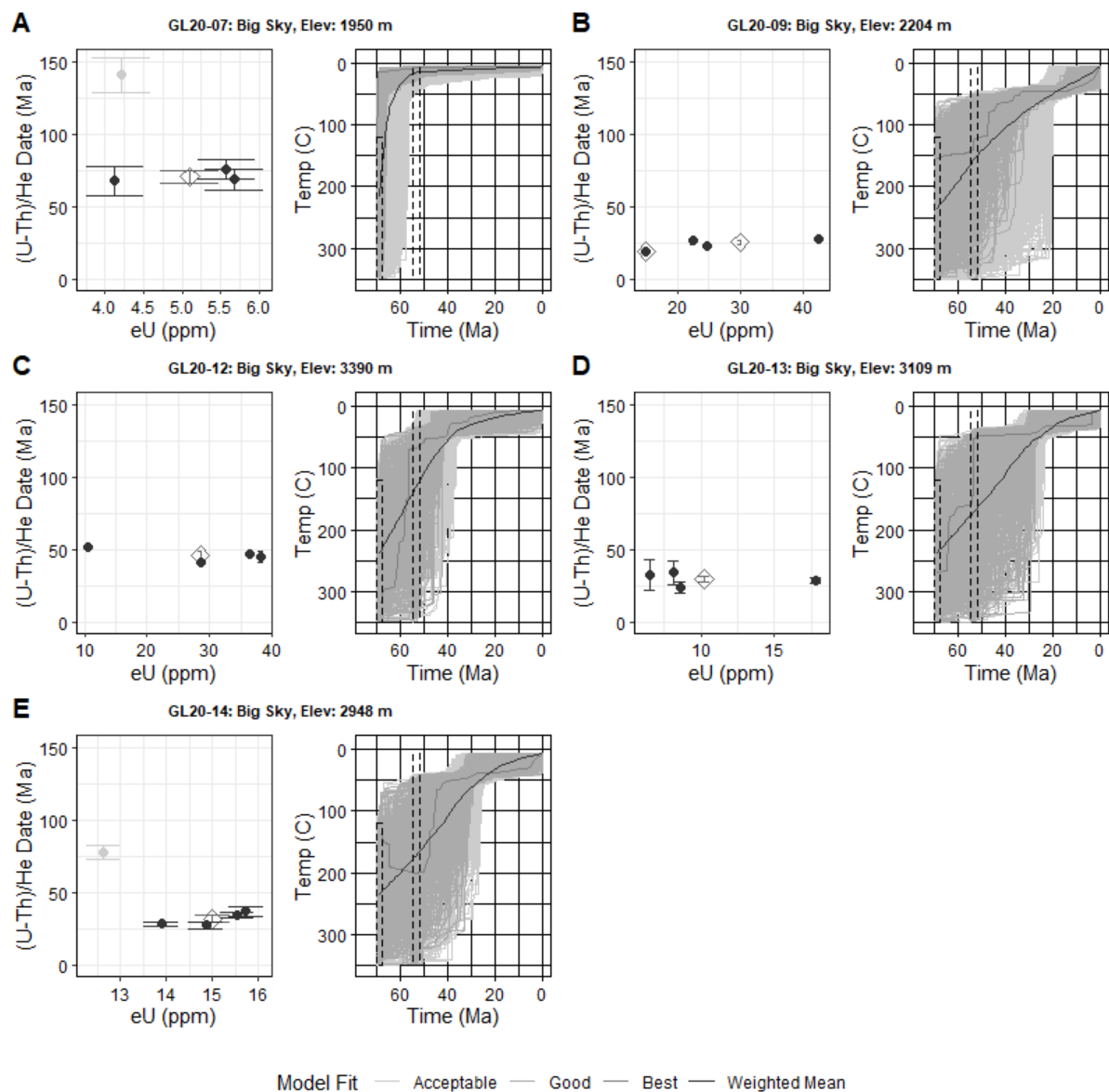


Fig. 4: (A-E) AHe eU and thermal modeling results for all samples in the Big Sky transect with <20% dispersion (standard deviation divided by the sample mean). Symbols and definitions are the same as Figure 3.

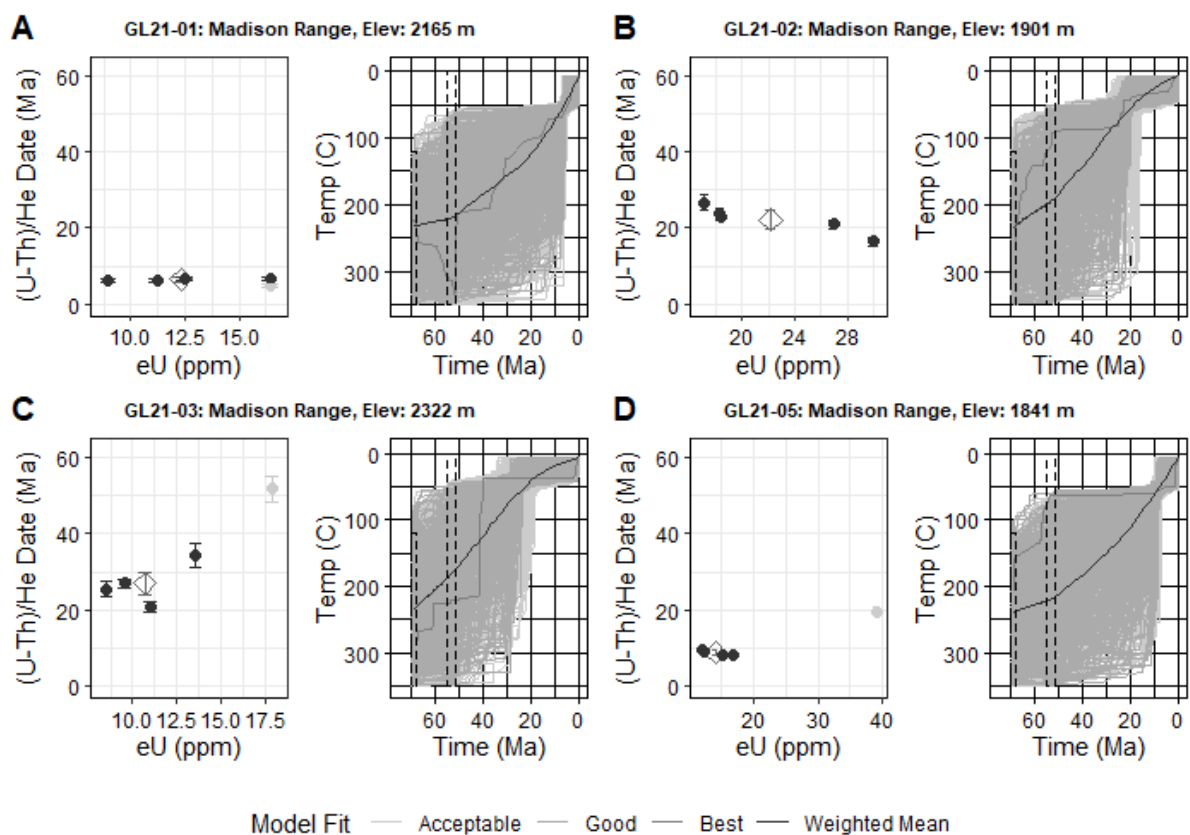


Fig. 5: (A-D) AHe eU and thermal modeling results for all samples in the Madison Range transect with <20% dispersion (standard deviation divided by the sample mean). Symbols and definitions are the same as Figure 3.

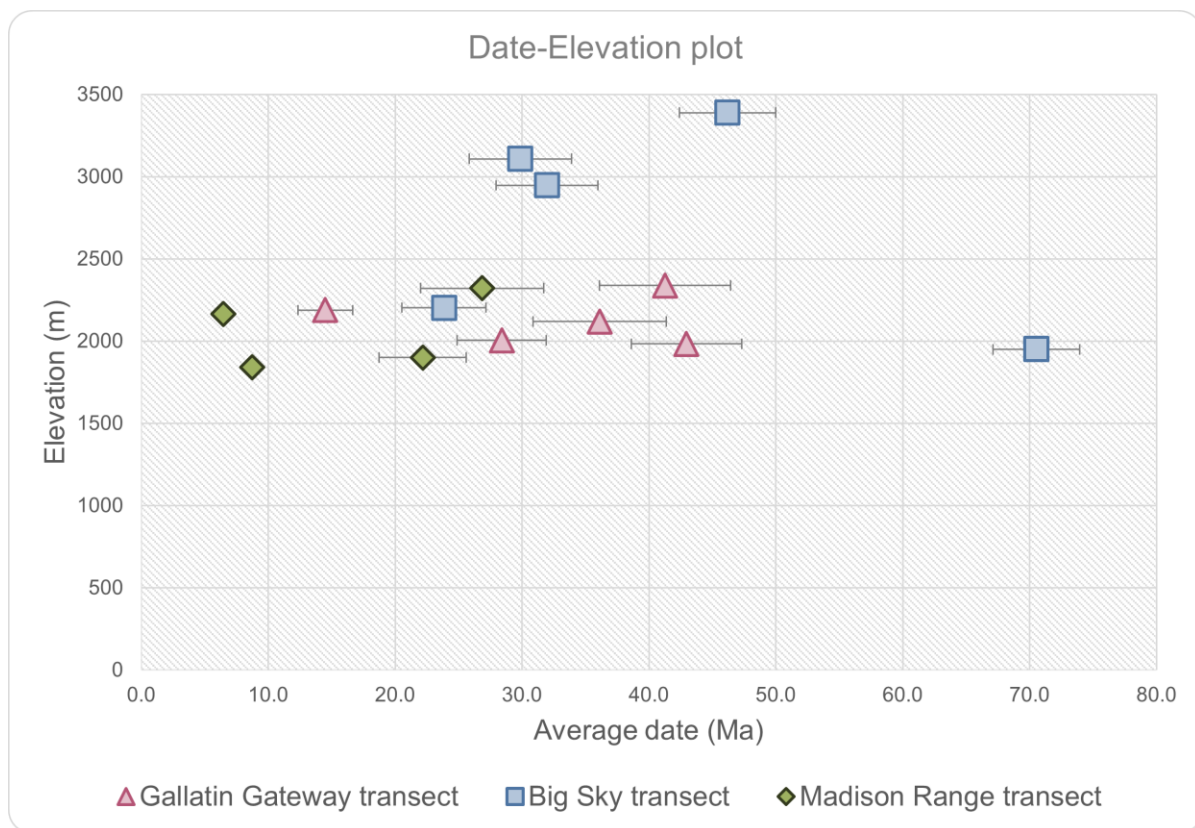


Fig. 6: Average AHe cooling dates plotted against elevation for all three transects (Gallatin Gateway plotted in pink triangles, Big Sky plotted in green squares, and Madison Range plotted in purple diamonds). Standard deviation for each sample is plotted as error bars and may be obscured by symbols.

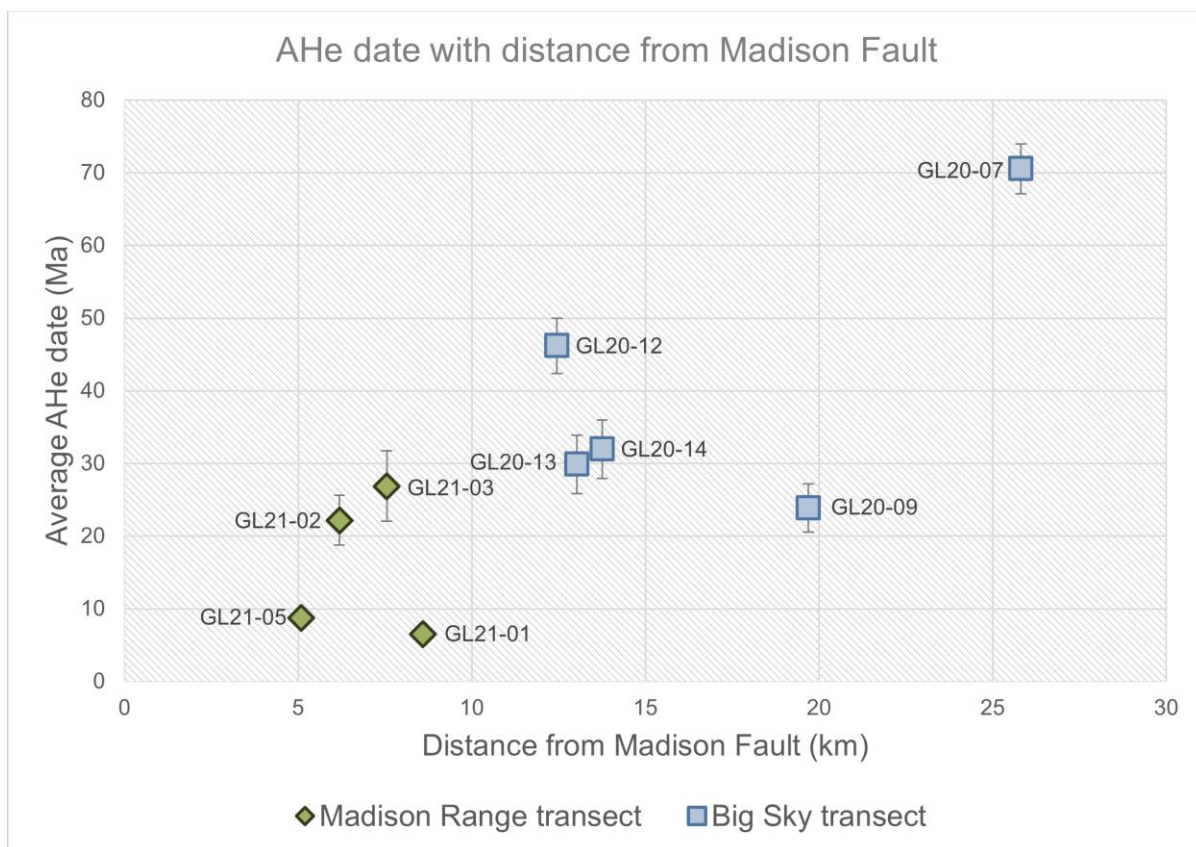


Fig. 7: Average AHe cooling dates for the Madison Range and Big Sky transects plotted against distance from the Madison Fault (Figure 1, 2). Standard deviation for each sample is plotted as error bars and may be obscured by symbols.

Inverse Modeling Results

Inverse modeling plots for the Gallatin Gateway, Big Sky and Madison Range transects are shown in Figures 3-5. For discussing thermal history modeling results, we will focus on the times that good-fit paths from samples are passing through the apatite partial retention zone (PRZ), ~90-40°C (Wolf et al., 1998; Farley, 2000; Ehlers and Farley, 2003; Flowers et al., 2009). This temperature represents the window where the AHe system is most sensitive. HeFTy modeling results show variable cooling trends across all samples. For most samples, good-fit t-T paths show wide envelopes prior to the earliest date of cooling suggesting numerous paths at variable speeds of cooling are plausible. However, none of these paths cool to <40°C immediately after emplacement, with the exception of sample GL20-07 in the Big Sky transect (Fig. 4). GL20-07 instead shows similar steep t-T paths that cool through the PRZ to near-surface temperatures almost immediately after

emplacement, suggesting this sample is required to cool quickly following emplacement.

For the majority of samples that do not cool immediately following emplacement, we can examine the amount of time each sample spends within the PRZ by looking at the latest time each sample is allowed to cool below $\sim 90^{\circ}\text{C}$ and the earliest date it is allowed to cool below $\sim 40^{\circ}\text{C}$. Most samples are allowed to pass through the PRZ quickly at a time that overlaps with their average AHe date, and many require at least some cooling during that window (Fig. 3-5). Except for samples GL20-01 and GL20-09, the latest date all paths enter the PRZ is younger than the earliest date they can exit the PRZ, meaning that they can cool through the PRZ very quickly. Samples GL20-01 (Fig. 3) and GL20-09 (Fig. 4) differ from the others in that they are required to spend some time in the PRZ. For GL20-01, the latest this sample can cross into the PRZ at 90°C is at ~ 42.5 Ma, and the earliest it can cross over at 40°C is not until ~ 12.5 Ma. At its fastest cooling, this sample is required to spend ~ 30 Ma in the PRZ before it is allowed to cool to surface temperatures, with some paths allowing for longer. Similarly, sample GL20-09 is also required to spend ~ 10 Ma in the PRZ.

An additional constraint was added to each inverse model across all transects representing a possible reheating event related to the eruption of the Absaroka Volcanic Province, which would allow samples to reach temperatures between ~ 300 - 350°C from ~ 55 - 52 Ma (Table 2; Chadwick, 1969; Feeley, 2003; Kellogg and Harlan, 2007). Modeled t-T paths were allowed to reheat during this time frame but were not required to. This event is reflected in some t-T paths which show samples reheating during this time, however none of the envelopes for any samples required reheating during this phase. Sample GL20-07 does not allow reheating during this time, and other samples do not have the ability to constrain this reheating phase.

Discussion

Post-Laramide Cooling in the Northern Madison and Gallatin Ranges

The AHe dates and inverse modeling presented in this study provide new constraints on the timing of post-Laramide cooling in this region. By targeting Tertiary-Cretaceous aged intrusions, our

AHe data isolates cooling histories that record lower magnitude exhumation after the events of the Laramide. Previous thermochronometer work in the area has explored regional cooling histories, but those studies targeted older lithologies that are not as sensitive to lower magnitude cooling and were largely focused on Laramide cooling and interpretations (Carrapa et al., 2019; Kaempfer et al., 2021). This study works to fill the temporal gap between those cooling history narratives and Cenozoic drivers of landscape evolution in southwest Montana.

Our AHe analyses produced a range of dates across three transects from 70 ± 3.4 Ma to 6.4 ± 0.28 Ma (Table 1). All sample dates are considerably younger than their inferred emplacement age except for one sample in the Big Sky transect (GL20-07) whose AHe date may be reflecting the emplacement age for our sampled intrusions (69 ± 1 Ma, Tysdal, 1986). Excluding this sample, the oldest AHe date is ~ 23 Ma younger than its age of emplacement. HeFTy inverse modeling of these samples shows that none of the samples are allowed to cool rapidly to surface temperature after emplacement (Fig. 3-5). This indicates that some cooling is the result of exhumation rather than simply post-magmatic cooling.

The Big Sky transect spans the largest elevation range and is also the only transect to show a correlation between AHe date and elevation. Four out of six samples show a positive correlation between date and elevation ranging from ~ 25 -46 Ma over 1186 m of relief (Fig. 6). This trend suggests that during this time, samples in this transect may have been continuously exhumed with either steady or increasing relief. This means the highest elevation sample in this transect cooled through the PRZ before the lowest elevation sample, and we can observe older dates at higher elevations and younger dates at lower elevations, which would be expected if the crustal block is exhuming steadily through the PRZ and isotherms are not affected by decreasing relief (e.g., Braun, 2002). A fifth sample from the transect is dispersed and the AHe date for the lowest sample in the transect is anomalous in that it is the oldest sample in the transect with an AHe date that overlaps with its probable emplacement age (GL20-08, GL20-07; Table 1). The t-T paths for the oldest sample show rapid cooling following emplacement and suggests this sample is not recording exhumation like

the other samples in this transect. For this reason, we do not interpret it with the other samples that are recording exhumation.

The Gallatin Gateway samples were also collected as an elevation transect but cover a smaller range of elevations. Limitations in the availability of intrusion outcrops and general topographic relief of the area resulted in a 355 m difference in relief between samples of the lowest and highest elevation. Although these samples are slightly more clustered, AHe dates produced a range of dates from ~43-14.5 Ma (Table 1). Plots for AHe date versus elevation did not show any obvious trend for this transect and dates are generally older compared to dates of the Big Sky transect at similar and higher elevations (Fig. 5). An exception to this is sample GL20-01, this sample has an anomalously young date of ~14.5 Ma with a similar elevation to other samples within this same transect.

The motivation for sampling in the Madison Range transect was to quantify any trend between distance to the Madison Fault to assess any impact of fault motion on cooling. These samples were collected as a horizontal transect and have a limited range of elevations with AHe dates that range from ~27-6.5 Ma (Table 1). Plotting each sample AHe date with distance to the Madison Fault does not show any obvious trend across all samples but there are three samples which do increase in date with increased distance from the fault (Fig. 7). Sample GL21-01 is one of the furthest samples from the Madison Fault, has the youngest date in the transect, and does not align with this potential trend. This sample is located on the footwall of an inferred normal fault to the east of the main Madison Fault system (Vuke, 2013). There are limited constraints on this fault apart from its possible location and slip sense, but it may be possible minor movement along this fault and/or fluid flow along the fault plane influenced this anomalous date. When considered with the Big Sky transect just east of the Madison transect (Fig. 2), it does appear there might be a relationship where cooling ages are older moving away from the Madison Fault (Fig. 7), but the wide range in elevation may also play a role in this trend. Overall, samples in the Madison Range transect are younger than sample dates in the Gallatin Gateway transect at similar elevations and overall younger than samples in the Big Sky

transect but could be a continuation of the age-elevation relationship from that transect given the proximity of the Big Sky and Madison transects (Fig 6, Fig 2). Overall, this suggests that the Madison Fault contributes to exhumation of samples close to the fault, but the total impact is difficult to disentangle from the effects of elevation differences.

To make general comparisons between the transects and look for date clusters, we plotted all the individual AHe dates for grains from each transect as kernel density estimates (KDEs) using the average value of all individual grain uncertainties as the bandwidth (Fig. 8). A KDE is an analytical tool used to observe the distribution of values within a dataset with the highest probable values represented as peaks. Plotting individual grain dates this way may help identify possible peaks within our dates that represent more significant periods of cooling. It is important to note that the non-parametric nature of kernel density estimations makes them blind to any specific spatial patterns or controls on dates, and that this method is used here purely as a tool for general comparison. Interpreting these KDEs also implicitly assumes our AHe dates are directly representative of the time each sample cooled through the PRZ. Examining the HeFTy models, the majority of paths for most samples have relatively short residence times in the PRZ which overlaps with average AHe dates for the sample. This suggests that the AHe date is often representative of the time at which samples have cooled through the PRZ. It is reasonable then to interpret the AHe date directly as the time of cooling for each sample, but we acknowledge this is not always the case.

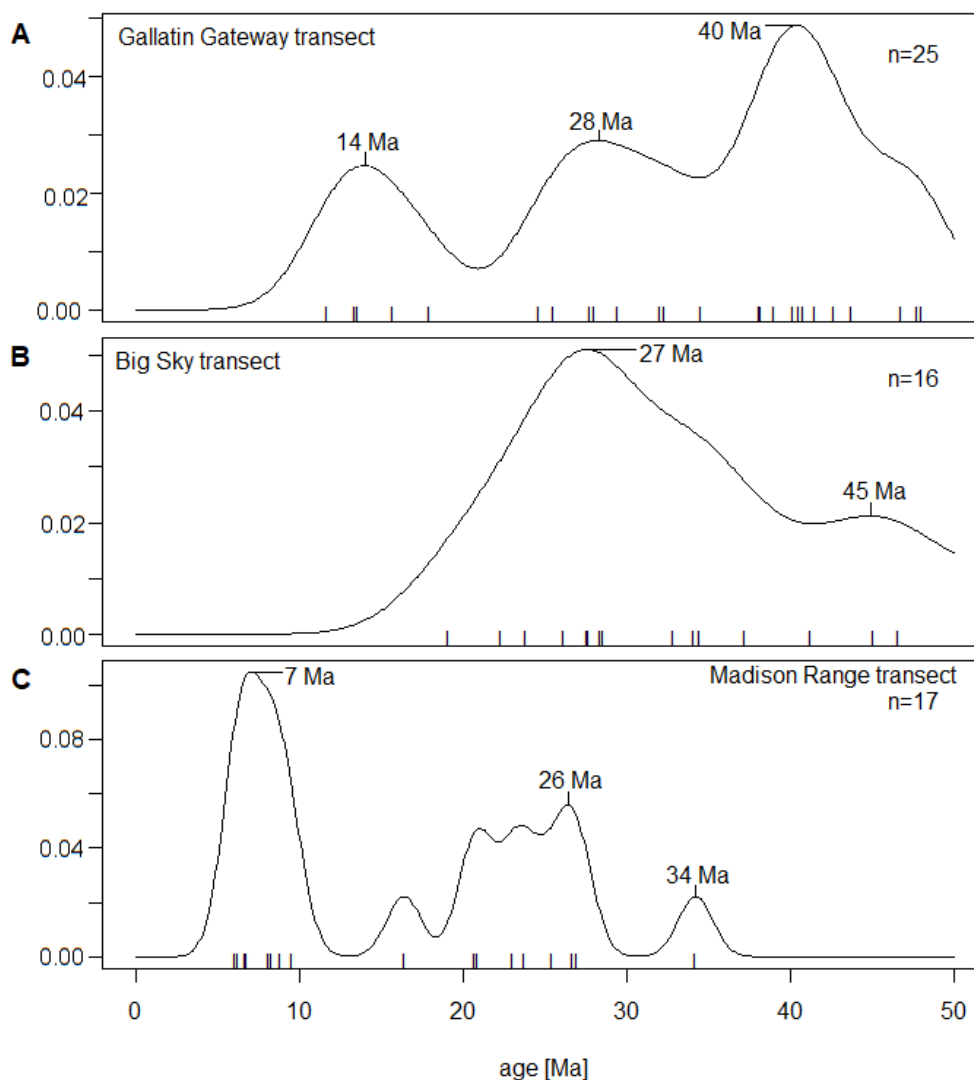


Fig. 8: (A-C) Kernel density estimate (KDE) plots of AHe cooling dates for the Gallatin Gateway, Big Sky and Madison Range transects. Bandwidth for each plot is the average 2σ uncertainty of individual grain dates (Gallatin Gateway = 2.37, Big Sky = 3.13, Madison Range = 1.06). Samples were plotted using R package ‘provenance’ v3.3 (Vermeesch et al., 2016).

KDE plots for each transect show there are observable peaks and similarities within samples (Fig. 8). Distributions from all three transects have similar peaks at ~26, 27, and 28 Ma. The Gallatin Gateway and Big Sky have another nearly overlapping peak at ~40 and 45 Ma. Similarly, the Gallatin Gateway and Madison Range transects have a nearly overlapping peak at ~13 and 15 Ma.

Paleocene Cooling

Many of the AHe dates for the Gallatin Gateway and Big Sky transects are Eocene and Oligocene. The date-elevation relationship in the Big Sky transect suggests continuous exhumation

from ~45 to 25 Ma (Fig. 6) and transect KDEs show peaks at ~27, 40, and 45 Ma (Fig. 8), overall showing Eocene and Oligocene cooling. The Madison Range transect also has AHe dates and KDE peaks in the late Oligocene to the early Miocene including peaks from ~21-26 Ma that coincide with two AHe dates within this same range (Table 1). Analysis of our date-elevations plots shows that although the Gallatin Gateway does not appear to exhibit any obvious trend, the Big Sky transect has a more convincing positive slope indicating there is some relationship between age and elevation which may be interpreted as steady exhumation over the period from ~25-45 Ma, the dates that bracket the positive trend. It is possible we do not see this trend in the Gallatin Gateway because those samples do not span a large enough elevation range to show a clear relationship. As a longer vertical profile, the date-elevation plot in Big Sky suggests that there may be continuous exhumation with steady or increasing relief because we can observe older dates at higher elevations and younger dates at lower elevations as is expected with a positive date-elevation slope (Braun, 2002).

Following the Laramide, the Cordilleran orogenic wedge was in an overthickened state due to extensive compression during the Sevier and Laramide Orogenies. In addition to high topography from thickened crust, magmatism from the onset of extension may have contributed to additional uplift through crustal thickening from added material, thermal expansion from surrounding bedrock, and changes in pressure within magma chambers (Fernández and Rundle, 1994, Van Wijk et al., 2016). An increase in topography during the Eocene is consistent with several studies focusing on paleotopographic reconstruction using $\delta^{18}\text{O}$ stable isotopes. These all support a general north-south increase in topography along the length of the fold and thrust belt coeval with post-Laramide extension and magmatism. A synthesis of both new and existing $\delta^{18}\text{O}$ and $\delta^{13}\text{C}$ stable isotope data from southwest Montana shows an increase in surface elevation ≥ 4 km from ~55-50 Ma following a period of increased relief within the Sevier fold and thrust belt from ~58-53 Ma (Schwartz et al., 2019). A 7-10‰ negative shift in $\delta^{18}\text{O}$ values from ~50-47 Ma in western Montana and east-central Idaho is interpreted as a surface elevation increase of 2.5-3.5 km coincident with the initiation of Challis magmatism at ~50 Ma to the west (Kent-Corson et al., 2006). Overall surface uplift through

the length of the fold and thrust belt may be attributed to delamination of the mantle and/or breaking of the Farallon slab (Constenius et al., 2003), however evidence would suggest that changes to topography also occurred near regions of extensional magmatism such as what is described in Kent-Corson et al. (2006) for regions near the Challis Volcanic Province.

Contemporaneous Absaroka magmatism in the east may have had a similar influence on topography at the time resulting in unroofing from erosion driven exhumation in those areas heavily affected by the Absaroka eruptions. Within our study area, this is the Gallatin Range and perhaps to a lesser extent the Madison Range to the west. Magmatism from the Absaroka Volcanic Province began at the onset of major extension and lasted from ~55-44 Ma with the portion that extended north into and throughout the Gallatin Range lasting from ~55-52 Ma (Feeley, 2003). This period of magmatism slightly pre-dates the oldest AHe dates in the Gallatin Gateway and most of the dates in the Big Sky, but these dates may be indicative of more indirect Absaroka influences on cooling in the time following eruption (Fig. 9). There are limited constraints on the thickness of Absaroka intrusives within the Gallatin Range, but Absaroka magmatism was voluminous across southwest Montana and Wyoming. Rocks of the Absaroka eruption are widespread in the Gallatin Range and east of the Gallatin River, but outcrops are extremely limited to the west towards the Madison Range (Kellogg and Williams, 2007). This limits any possible influence on AHe dates in Big Sky unless evidence of magmatism towards the west has been subject to erosion. The volume of magma concentrated in the

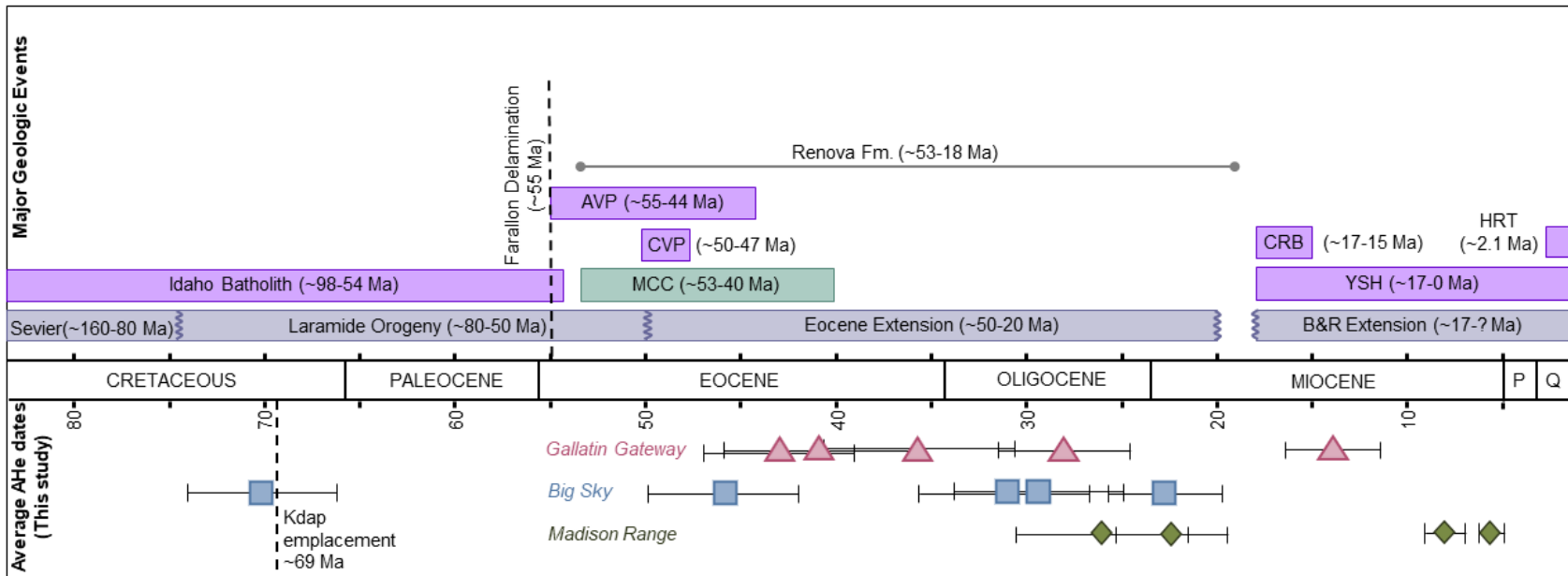


Fig. 9: Timeline diagram depicting generalized major geologic events within the Cordillera Orogenic system. References cited within the text. AHe dates from this study are presented at the bottom for each whole transect. Standard deviation for each sample is plotted as error bars and may be obscured by symbols. Abbreviations: AVP – Absaroka Volcanic Province, B&R Extension – Basin and Range Extension, CRB – Columbia River Basalts, CVP – Challis Volcanic Province, HRT – Huckleberry Ridge Tuff, Kdap – Cretaceous dacite porphyry, MCC – Metamorphic Core Complexes, P – Pliocene, Q – Quaternary, Renova Fm. – Renova Formation, YSH – Yellowstone Hotspot.

Gallatin Range may have encouraged gradual regional uplift and exhumation from erosion during eruption and intrusion recorded in the oldest dates and KDE peaks at ~45-40 Ma in the Gallatin Gateway and Big Sky transects. The volume of magmatism may have also had additional thermal effects on our dates through reheating, however this would depend on the proximity to Absaroka volcanics. It is also worth noting that sample GL20-05 in the Gallatin Gateway is mapped as an Absaroka related intrusion and has an average AHe date of 42.96 ± 2.13 Ma (Table 1). If this sample was emplaced during Absaroka magmatism, then the <55-52 Ma date may support post-emplacment exhumation.

The eventual gravitational collapse of the thickened orogenic wedge led to extension during the Eocene in the hinterland of the Sevier fold and thrust belt within western Montana and central Idaho that lasted until ~20 Ma (Constenius, 1996). Early evidence of extension in this region is visible by the presence of widespread normal faulting in east-central Idaho which began ~48-46 Ma, contributing to the formation of extensional basins from the middle Eocene through the Oligocene (Janecke, 1992). Basin formation is coeval with Challis magmatism from ~50-47 Ma and the development of the Anaconda and Bitterroot metamorphic core complexes from ~53-44 Ma (Constenius, 1996; Sears and Ryan, 2003; Janecke, 2007; Schwartz et al., 2019). Any direct influence on our study area from these processes is unlikely due to distance, however the demonstrable evidence for Eocene extension in the west along the length of the fold and thrust belt shows that the magnitude of extensional stress was substantial. Although there is no evidence for larger extensional structures such as metamorphic core complexes further east near our study area, the cooling signal we observe in our dates may be reflecting this reach as minor exhumation from more brittle extension on the easternmost boundary of major extension. Contemporaneous evidence of extension in the Laramide foreland is recorded in the sedimentary record of the Renova Formation in basins just to the west and north of our study area (Fig. 1; Kuenzi and Fields, 1971; Hanneman and Wideman, 1991; Fritz and Sears, 1993; Vuke et al., 2002; Schwartz and Schwartz, 2013). This formation is the earliest proposed record of post-compressional sedimentation and is considered synextensional basin-fill

(Kuenzi and Fields, 1971; Hanneman and Wideman, 1991). It is comprised of numerous individual units/members that were deposited from ~53-18 Ma (Fig. 9; Constenius, 1996; Schwartz et al., 2019). Several basins surrounding our study area, including the Jefferson, Upper Ruby, Three Forks, Clarkston, and Townsend basins (Fig. 1), record outcrops of the same Renova Formation, suggesting synextensional deposition was occurring at similar times in areas of similar longitudes to our study area (Robinson and Barnett, 1963, Kuenzi and Fields, 1971; Hanneman and Wideman, 1991). The timing of Renova deposition for the Jefferson, Three Forks, Townsend and Clarkston Basins is from ~37-31.8 Ma based on North American Land Mammal Ages (NALMA) (Kuenzi and Fields, 1971). The Renova is up to 520 m thick in parts of the Upper Ruby Basin and up to 294 m thick north in the Jefferson Basin (Kuenzi and Fields, 1971; Monroe, 1981). In addition to Renova deposition, Robinson (1961) mentions an Eocene deposited limestone conglomerate in the western half of the Three Forks Basin that resembles the Sphinx conglomerate of the Madison Valley (Robinson and Barnett, 1963). The Maastrichtian aged Sphinx conglomerate type unit originates within the Madison Range atop Sphinx Mountain and Helmet Peak (DeCelles et al., 1987). Apatite fission track data for a volcanic clast within the Sphinx conglomerate yielded a date of $\sim 41.5 \pm 3.2$ Ma (Carrapa et al., 2019) supporting Eocene cooling in the Madison Valley in addition to serving as a possible sediment source for the Sphinx conglomerate in the Three Forks basin. The temporal overlap between basin deposition and our cooling dates may suggest that extensional processes are driving topographic uplift and exhumation during the Paleocene visible in the t-T paths of our samples.

Our AHe dates in the Eocene and Oligocene for the Gallatin Gateway, Big Sky and Madison Range transects in combination with modeled t-T paths and KDE date peaks show evidence for Paleocene cooling. These signals and evidence for the topographic conditions at the time indicates there are potentially several interconnected mechanisms at work influencing cooling in the region. The transition from compressional to extensional stress in the early Eocene resulted in extensional collapse of the Cordilleran orogenic wedge that propagated west until ~20 Ma producing both widespread extension and magmatism (e.g., Constenius, 1996; Yonkee and Weil, 2015). Large-scale

Eocene extension to the west was accompanied by extensive volcanism (i.e., Challis Volcanic Province), the formation of core complexes, and synextensional basins (Fig. 9; Kuenzi and Fields, 1971; Hanneman and Wideman, 1991; Janecke, 1992; Constenius, 1996; Sears and Ryan, 2003; Janecke, 2007; Schwartz et al., 2019). Studies of paleotopographic reconstruction in southwest Montana support a period of high topography from ~58-47 Ma (Kent-Corson et al., 2006; Schwartz et al., 2019). While our study area is not close enough to be directly influenced by these processes, it sits in what may be an eastern edge of extension and rapid collapse. An increase in relief to the east associated with collapse to the west is consistent with the trend of continuous exhumation with either steady or increasing relief we observe for samples in Big Sky from ~45-25 Ma (Fig. 6). Influence of the Absaroka Volcanic Province on regional surface uplift may have encouraged exhumation and erosion in the Gallatin Gateway much like observed surface uplift in regions surrounding the Challis Volcanic Province in the west (Kent-Corson et al., 2006; Chetel et al., 2011). Evidence of the synextensional Renova Formation in basins just north of our study area suggests that extensional sedimentation also extended east (Robinson and Barnett, 1963, Kuenzi and Fields, 1971; Hanneman and Wideman, 1991). The associated isostatic uplift from collapse together with dynamic and thermal uplift from extension and Absaroka magmatism may each be contributing in part to the exhumation history of our samples in the Gallatin Gateway and Big Sky transects resulting in gradual exhumation triggered by increasing topography and erosion.

Madison Fault Driven Exhumation

The Madison transect overall yielded younger AHe dates with two samples having Miocene ages (Table 1). These young dates post-date any signal from Eocene processes meaning exhumation must originate from another source, and the nearby Madison Fault presents a likely source of cooling. The Madison Fault extends 98 km in length and is sectioned into moderately constrained northern, central, and southern portions that have been active throughout the Quaternary (Haller et al., 2000). Information regarding the origin of the Madison Fault and the history of its movement beyond the

Quaternary is limited (Pardee, 1950; Anders et al., 1989), however one source suggests it may have been produced by Tertiary extension with normal slip sense (Trimble and Smith, 1975). The most recent record of movement along this fault occurred during the 1959 Hebgen Lake earthquake but evidence of westward dipping faults, both new and reactivated, along the YCHT suggests this fault may have been active in the Eocene through the passage of the YHS to the present with a total maximum throw of ~8 km (Haller et al., 2000; Pierce and Morgan, 2009). Evidence for movement along the southern portion of the Madison Fault is better constrained and would suggest it has been continually active with estimated quaternary recurring intervals of activity every ~10-25 Ka (Haller et al., 2000). The constraints on movement along the Madison Fault, particularly those in the northern section closest to our Madison Range transect, are significant to our cooling dates. Figure 8 shows the Madison Range AHe dates plotted against approximate distance to the Madison Fault. The closest sample to the fault, ~5km away is one of the youngest cooling in our sample suite at ~9 Ma and broadly dates get older away from the fault. Additionally, an average AHe date of $\sim 21.2 \pm 0.6$ Ma from another study is reported for a bedrock sample from Sphinx Mountain which is directly south from our Madison Range transect along the Madison fault and consistent with other dates within that transect (Carrapa et al., 2019). This proximity, the recurrence of activity, and the considerable amount of overall displacement along the length of the fault makes it a likely source of Miocene cooling by fault-driven exhumation for samples in the Madison Range (Fig. 5).

One sample in the Gallatin Gateway (GL20-01) has an anomalously young AHe date of ~14.5 Ma and is one of the youngest dates in this study. The AHe date would suggest the source of cooling for this sample is either extremely localized or event specific. It is difficult to determine the source of cooling at this time without further speculation and our data is limited in its ability to fully explain this sample date.

The youngest AHe dates in the Madison Range are late Miocene and patterns of AHe dates are indicative of cooling driven by the Madison Fault to the west. The magnitude of movement along the fault and other well constrained evidence of fault activity makes it an appropriate and probable

source of cooling from fault driven exhumation for samples in this transect. The older two samples in the Madison transect may be reflecting a combination of Eocene exhumation and contribution from more recent Madison Fault motion. Exact timing of fault motion is not known and difficult to constrain specifically from our data but offset 2 Ma Huckleberry Ridge tuff in the central portion of the fault by 800-900 m (Pierce and Morgan, 1992) suggests 0.4 mm/yr of motion. If total maximum throw is 8 km (Locke and Schneider, 1990; Haller, 2010) then the fault could have been active since ~20 Ma if the rate of motion was continuous throughout its history.

Yellowstone Hotspot Influence on Cooling

All of our AHe dates pre-date the arrival of the Yellowstone hotspot (YSH) to its current location, marked by the eruption of the Huckleberry Ridge Tuff at ~2.0 Ma (Fig. 9; Pierce and Morgan, 1992). Our youngest AHe date is 6.5 ± 0.28 Ma which pre-dates the Huckleberry Ridge tuff by 4.5 Myr (Table 1). None of our samples require erosion after 2 Ma, meaning the landscape's erosional response to any YHS uplift has been fairly limited, but most samples do allow for some cooling during this window (Fig. 3-5). The maximum amount of cooling allowed by all samples according to our good-fit HeFTy t-T paths between ~2.0-0 Ma is ~24-49°C (Fig. 3-5). Samples of the Madison Range allow for a greater range of maximum cooling across all samples from ~39-49°C compared to Big Sky which allows for ~29-39°C and lastly the Gallatin Gateway which only allows ~24°C of cooling (not including sample GL20-01 which allows ~49°C of cooling). Using estimates for the geothermal gradient, we can use these amounts of maximum cooling to help establish an upper limit of how much exhumation from additional cooling may be possible with the arrival of the hotspot. Prior to the arrival of the hotspot, the geothermal gradient would be that of normal continental crust with an estimated temperature of ~25°C/km (DiPietro, 2013). The range of possible exhumation after ~2.0 Ma based on this model would be between ~0.72-1.72 km. However, the arrival of the hotspot has altered the surrounding geotherm with the addition of heat from the mantle plume. Based on this, estimates for the geothermal gradient at present are slightly higher than that of

normal continental crust. In our study area, the geotherm has increased since the arrival of the hotspot to $\sim 30^{\circ}\text{C}/\text{km}$ (Blackwell et al., 2011; Gunderson, 2011). Assuming this temperature is uniform throughout our study area, samples in each of our transects may be restricted to between ~ 0.60 - 1.43 km of exhumation at their highest approximate amount of additional cooling. Samples in the Madison Range are allowed ~ 1.10 - 1.43 km of exhumation, followed by Big Sky with ~ 0.77 - 1.10 km, and Gallatin Gateway with ~ 0.60 km.

Based on established evidence of deformation and topographic evolution contributed through dynamic and thermal processes (Waschbusch and McNutt, 1994; Sears and Thomas, 2007; Smith et al., 2009) within the Yellowstone Crescent of High Terrain (YCHT) (Anders and Sleep, 1992; Fritz and Sears, 1993; Rogers et al., 2002; Beranek et al., 2006; Pierce and Morgan, 2009; Sears et al., 2009; Vogl et al., 2014) and along the Eastern Snake River Plain (ESRP) (Suppe et al., 1975; Brott et al., 1981; McQuarrie et al., 1988; Anders et al., 1989; Rodgers et al., 1990; Rodgers et al., 2002), we originally hypothesized that the arrival of the hotspot would have a more significant contribution to cooling in this region. The inception of the Heise Volcanic field at ~ 6.62 Ma just southwest of our study area caused segmentation of paleo-valleys leading to proposed changes to paleo-drainage routes at ~ 6.5 Ma. This change to topography suggests that the hotspot's progression facilitated deformation in pre-existing basins as well as re-organization of fluvial drainage away from developing high topography (Fritz and Sears, 1993; Pierce and Morgan, 2009; Camp and Wells, 2021; Staisch et al., 2021). It is reasonable to consider then that inception of magmatism at the hotspot's current location at the Yellowstone plateau would trigger a similar response. Contrary to this, the youngest AHe dates in our data suggests samples cooled through the PRZ to surface temperatures prior to the arrival of the hotspot to its current location. This suggests that any contribution from the most recent volcanic center to exhumation and/or surface uplift from changes to topography and erosion is minimal. Since the Heise caldera is directly south of our study area, it may be reasonable to expect cooling due to uplift from the Heise caldera or during the transition period from the Heise to the Yellowstone plateau, and our youngest AHe date does overlap with Heise caldera activity. However, proximity of

these young dates to the Madison Fault suggests exhumation is controlled by fault processes rather than regional uplift.

The lack of substantial rock uplift and exhumation from the hotspot in our data contrasts previous work along the hotspots track that shows evidence of hotspot motivated changes to topography that drove exhumation. Previous thermochronometry work by Vogl et al. (2014) in the Pioneer-Boulder Mountains identifies surficial changes from hotspot processes as the primary source of exhumation and uplift with over 2-3 km of exhumation since ~11 Ma with limited evidence of fault driven exhumation from extension. The amount of exhumation in this study exceeds what's possible in our study area even with a "normal" geothermal gradient. It is possible the differences in outcome of this study and ours can be explained by the inherent differences between each study area. Our study area lies much further east towards the North American craton with a crustal thickness of $\sim >44$ km compared to that of the Pioneer-Boulder Mountains with a thickness of $\sim 36-38$ km (Gilbert, 2012). The interaction of the mantle plume with thicker continental crust may be affecting uplift and exhumation. Presumably the same hotspot processes on thickened crust would produce less exhumation from the upward force required to incite uplift. Another potential source of variation is the timing of the hotspot's progression through each region. The Pioneer-Boulder Mountains are in central Idaho north of the Twin Falls (12.7-8.5 Ma) and Picabo (10.3-8.2 Ma) Calderas. The ESRP and these two calderas have been subject to considerable subsidence since the passing of the hotspot which has not yet occurred in our study area. Instead of exhumation driven by thermal uplift and erosion, it's possible the significant amount of exhumation measured in the Pioneer-Boulder Mountains is the result of exhumation driven by the flexural-isostatic response to subsidence in that portion of the ESRP (e.g., McQuarrie and Rodgers, 2002), much like we see in the region of high topography surrounding the plain (YCHT). If this is the case, then our young AHe dates may be showing that there is more exhumation with the progression of the hotspot from collapse and subsidence than there is from dynamic topography and thermal uplift. Exhumation is therefore more readily observed in places such as faults where movement is more easily achieved as is evidenced by

our youngest AHe dates close to the Madison Fault.

The Madison Fault appears to play a critical role in driving cooling in some of our samples. While this cooling likely does not reflect regional doming and uplift of the YCHT, activity on the Madison Fault may also be due to hotspot processes. Anders et al. (1989) proposed bands of active seismicity fanning out from the YHS with a similar pattern to the YCHT. The Madison Fault lies within the proposed “Belt II” of these seismic belts defined as areas of progressive fault activity coeval with hotspot migration and categorized as the region of peak fault activity from ~2.0-0 Ma (Anders, 1994; Pierce and Morgan, 2009). This is also supported by ~800-900 m of displacement of the Huckleberry Ridge Tuff (~2.0 Ma) along portions of the central Madison Range section, suggesting activity was prominent throughout the Quaternary (Pierce and Morgan, 1992; Haller et al., 2010).

Our AHe dates and HeFTy t-T paths show that although some cooling is allowed after ~2.0 Ma, the overall contribution to cooling in response to the arrival of the hotspot is subtle and may equate to ≤ 1.43 km of exhumation based on geothermal gradient estimations for our study area. Samples in the Madison Range suggest that there is greater impact on cooling from the Madison Fault by fault driven exhumation. It is difficult to quantify how much actual cooling and exhumation was influenced by the arrival of the hotspot either at the Heise caldera or Yellowstone plateau, but overall cooling from this source is minimal.

Conclusions

Bedrock thermochronology of elevation transects in the Madison and Gallatin Ranges of southwest Montana provide new AHe dates that record post-Laramide cooling and identify Cenozoic drivers of landscape evolution in this region. A positive spatial trend between AHe dates and elevation in Big Sky from the Eocene through Oligocene documents evidence for continuous exhumation with either steady or increasing relief (Fig. 6). Many AHe dates across the entire dataset are also Eocene to Oligocene in age. This is indicative of Paleocene cooling that may be influenced

by a variety of factors related to Eocene extension and magmatism (Fig. 9). Surficial uplift from the voluminous Absaroka Volcanic Province facilitated exhumation by erosion reflected in cooling dates in the Gallatin Range. Increased topography triggered erosional exhumation reflected in cooling dates for the Big Sky and Madison Range transects. These two transects are spatially far from the locus of major Eocene extension, but they help to constrain the reach of high topography produced by the isostatic response to western extension and eventual collapse of the Cordilleran fold and thrust belt which led to uplift and exhumation in these regions.

AHe dates from the late Oligocene to the Miocene show cooling continued following Eocene extension and collapse. The Madison Fault to the west of our Madison Range transect is the most likely source of cooling facilitated by fault driven exhumation. Evidence for the Madison Fault as the primary driver of exhumation for samples in the Miocene is reflected in our youngest AHe dates. Overall contribution from the erosion due to regional uplift and doming from Yellowstone hotspot is minimal, though hotspot processes could be driving some of the Madison Fault activity.

Future Work and Outstanding Questions

There are some outstanding questions and room for additional work that if accomplished would build upon and strengthen this project. Our study area is relatively understudied, particularly after the events of the Laramide, and this work shows there are larger tectonic implications beyond hotspot processes.

Firstly, a source of some uncertainty lies in the emplacement age of our intrusions. Our targeted intrusions are very similar in lithologies and although it is reasonable to assume a similar intrusion history, more accurate crystallization ages for each individual lithology would provide better constraints for HeFTy inverse modeling. This may reduce uncertainties in modeling and produce better overall interpretations. HeFTy itself provides some uncertainty as it cannot model samples together as whole vertical transects. As an additional form of data interpretation, it may be useful to also model our samples using another program such as QTQt that has the capability to model samples

together as one transect. This may provide an interesting comparison for interpretation with HeFTy modeling.

Secondly, depending on the availability of units and outcrops, it would be worthwhile to extend these transects by collecting more samples increasing our overall sample size and allowing for more robust KDE plots for interpretation. The Madison Range transect would benefit from the addition of more samples towards the south approaching the ESRP along the length of the Madison Fault system. This may let us evaluate any differences in exhumational response along the fault and as samples approach the hotspot track. If the hotspot has truly had a minimal effect on exhumation from ~2.0 Ma to present, then perhaps we may see a similar result even with proximity to the ESRP. Additional east-west vertical transects collected to the south of our transects may provide an interesting comparison to the data and interpretations presented in this study. Since our samples have already been separated for apatite, the addition of $^4\text{He}/^3\text{He}$ analyses may help to better constrain the lowest temperature portions of our thermal histories, particularly any possible cooling and exhumation after 2.0 Ma with the approach of the hotspot. Despite being an original motivator for this project, the YSH had less of an impact on exhumation than we expected. Part of this expectation stemmed from the numerous works of others whose results and interpretations showed that the hotspot plays a key role in exhumation and uplift along the hotspot track. It is possible the addition of more samples in our pre-existing transects may help to disentangle the differences in our data and explain the contrasting results of our study.

Lastly, a dominant piece of our interpretations identifies fault driven exhumation as a driver of cooling, particularly for the Madison Range transect which had the youngest AHe dates overall. However, it is difficult to isolate this from other sources of cooling such as erosion driven exhumation. Modeling the effects of normal faulting may work to verify whether the Madison fault is in fact influencing these young dates. Another potential avenue for evaluating movement along the fault may be conducting hematite (U-Th)/He analysis along portions of the Madison Fault both near

the Madison Range transect and further south towards the ESRP. This would require investigation into locations of possible fault exposures, which may be difficult given the densely vegetated nature of the region, but this would be an innovative way to quantitatively establish movement along the Madison Fault in addition to the magnitude of movement with proximity to the hotspot track.

References

- Anders, M.H., 1994, Constraints on North American plate velocity from the Yellowstone hotspot deformation field: *Nature*, v. 369, p. 53–55, doi:10.1038/369053a0.
- Anders, M.H., Geissman, J.W., Piety, L.A., and Sullivan, J.T., 1989, Parabolic distribution of circumeastern Snake River Plain seismicity and latest Quaternary faulting: Migratory pattern and association with the Yellowstone hotspot: *Journal of Geophysical Research: Solid Earth*, v. 94, p. 1589–1621, doi:https://doi.org/10.1029/JB094iB02p01589.
- Anders, M.H., and Sleep, N.H., 1992, Magmatism and extension: The thermal and mechanical effects of the Yellowstone Hotspot: *Journal of Geophysical Research: Solid Earth*, v. 97, p. 15379–15393, doi:10.1029/92JB01376.
- Armstrong, R.L., and Ward, P., 1991, Evolving geographic patterns of Cenozoic magmatism in the North American Cordillera: The temporal and spatial association of magmatism and metamorphic core complexes: *Journal of Geophysical Research: Solid Earth*, v. 96, p. 13201–13224, doi:10.1029/91JB00412.
- Beranek, L.P., Link, P.K., and Fanning, C.M., 2006, Miocene to Holocene landscape evolution of the western Snake River Plain region, Idaho: Using the SHRIMP detrital zircon provenance record to track eastward migration of the Yellowstone hotspot: *GSA Bulletin*, v. 118, p. 1027–1050, doi:10.1130/B25896.1.
- Blackwell, D., Richards, M., Frone, Z., Batir, J., Ruzo, A., Dingwall, R., and Williams, M., 2011, Temperature-At-Depth Maps For the Conterminous US and Geothermal Resource Estimates:, <https://www.osti.gov/biblio/1137036>.
- Braun, J., 2002, Quantifying the effect of recent relief changes on age–elevation relationships: *Earth and Planetary Science Letters*, v. 200, p. 331–343, doi:10.1016/S0012-821X(02)00638-6.
- Brott, C.A., Blackwell, D.D., and Ziagos, J.P., 1981, Thermal and tectonic implications of heat flow in the Eastern Snake River Plain, Idaho: *Journal of Geophysical Research: Solid Earth*, v. 86, p. 11709–11734, doi:10.1029/JB086iB12p11709.
- Brown, R.W., Beucher, R., Roper, S., Persano, C., Stuart, F., and Fitzgerald, P., 2013, Natural age dispersion arising from the analysis of broken crystals. Part I: Theoretical basis and implications for the apatite (U–Th)/He thermochronometer: *Geochimica et Cosmochimica Acta*, v. 122, p. 478–497, doi:10.1016/j.gca.2013.05.041.
- Brown, S.J., Thigpen, J.R., Spotila, J.A., Krugh, W.C., Tranel, L.M., and Orme, D.A., 2017, Onset Timing and Slip History of the Teton Fault, Wyoming: A Multidisciplinary Reevaluation: *Tectonics*, v. 36, p. 2669–2692, doi:10.1002/2016TC004462.
- Camp, V.E., and Hanan, B.B., 2008, A plume-triggered delamination origin for the Columbia River Basalt Group: *Geosphere*, v. 4, p. 480–495, doi:10.1130/GES00175.1.
- Camp, V.E., and Ross, M.E., 2004, Mantle dynamics and genesis of mafic magmatism in the intermontane Pacific Northwest: *Journal of Geophysical Research: Solid Earth*, v. 109, doi:10.1029/2003JB002838.
- Camp, V., and Wells, R., 2021, The Case for a Long-Lived and Robust Yellowstone Hotspot: *GSA Today*, v. 31, p. 4–10, doi:10.1130/GSATG477A.1.

- Carrapa, B., DeCelles, P.G., and Romero, M., 2019, Early Inception of the Laramide Orogeny in Southwestern Montana and Northern Wyoming: Implications for Models of Flat-Slab Subduction: *Journal of Geophysical Research: Solid Earth*, v. 124, p. 2102–2123, doi:<https://doi.org/10.1029/2018JB016888>.
- Chadwick, R.A., 1970, Belts of Eruptive Centers in the Absaroka-Gallatin Volcanic Province, Wyoming-Montana: *GSA Bulletin*, v. 81, p. 267–274, doi:[10.1130/0016-7606\(1970\)81\[267:BOECIT\]2.0.CO;2](https://doi.org/10.1130/0016-7606(1970)81[267:BOECIT]2.0.CO;2).
- Chadwick, R.A., 1969, The northern Gallatin Range, Montana, northwestern part of the Absaroka-Gallatin volcanic field: *Rocky Mountain Geology*, v. 8, p. 150–166.
- Chetel, L.M., Janecke, S.U., Carroll, A.R., Beard, B.L., Johnson, C.M., and Singer, B.S., 2011, Paleogeographic reconstruction of the Eocene Idaho River, North American Cordillera: *GSA Bulletin*, v. 123, p. 71–88, doi:[10.1130/B30213.1](https://doi.org/10.1130/B30213.1).
- Christiansen, R.L., 1984, Yellowstone magmatic evolution: Its bearing on understanding large-volume explosive volcanism: *Explosive Volcanism: Inception, Evolution, and Hazards*, p. 84–95.
- Christiansen, R.L., Foulger, G.R., and Evans, J.R., 2002, Upper-mantle origin of the Yellowstone hotspot: *GSA Bulletin*, v. 114, p. 1245–1256, doi:[10.1130/0016-7606\(2002\)114<1245:UMOOTY>2.0.CO;2](https://doi.org/10.1130/0016-7606(2002)114<1245:UMOOTY>2.0.CO;2).
- Coney, P.J., and Harms, T.A., 1984, Cordilleran metamorphic core complexes: Cenozoic extensional relics of Mesozoic compression: *Geology*, v. 12, p. 550–554, doi:[10.1130/0091-7613\(1984\)12<550:CMCCCE>2.0.CO;2](https://doi.org/10.1130/0091-7613(1984)12<550:CMCCCE>2.0.CO;2).
- Constenius, K.N., 1996, Late Paleogene extensional collapse of the Cordilleran foreland fold and thrust belt: *GSA Bulletin*, v. 108, p. 20–39, doi:[10.1130/0016-7606\(1996\)108<0020:LPECOT>2.3.CO;2](https://doi.org/10.1130/0016-7606(1996)108<0020:LPECOT>2.3.CO;2).
- Constenius, K.N., Esser, R.P., and Layer, P.W., 2003, Extensional Collapse of the Charleston-Nebo Salient and Its Relationship to Space-Time Variations in Cordilleran Orogenic Belt Tectonism and Continental Stratigraphy: , p. 303–353.
- Cooperdock, E.H.G., Ketcham, R.A., and Stockli, D.F., 2019, Resolving the effects of 2-D versus 3-D grain measurements on apatite (U–Th) and He age data and reproducibility: *Geochronology*, v. 1, p. 17–41, doi:[10.5194/gchron-1-17-2019](https://doi.org/10.5194/gchron-1-17-2019).
- DeCelles, P.G. et al., 1987, Laramide Thrust-Generated Alluvial-Fan Sedimentation, Sphinx Conglomerate, Southwestern Montana: *AAPG Bulletin*, v. 71, p. 135–155.
- DeCelles, P.G., 2004, Late Jurassic to Eocene evolution of the Cordilleran thrust belt and foreland basin system, western U.S.A.: *American Journal of Science*, v. 304, p. 105–168, doi:[10.2475/ajs.304.2.105](https://doi.org/10.2475/ajs.304.2.105).
- Dickinson, W.R., 2004, Evolution of the North American Cordillera: *Annual Review of Earth and Planetary Sciences*, v. 32, p. 13–45, doi:[10.1146/annurev.earth.32.101802.120257](https://doi.org/10.1146/annurev.earth.32.101802.120257).
- Dickinson, W.R., Klute, M.A., Hayes, M.J., Janecke, S.U., Lundin, E.R., McKittrick, M.A., and Olivares, M.D., 1988, Paleogeographic and paleotectonic setting of Laramide sedimentary basins in the central Rocky Mountain region: *GSA Bulletin*, v. 100, p. 1023–1039, doi:[10.1130/0016-7606\(1988\)100<1023:PAPSOL>2.3.CO;2](https://doi.org/10.1130/0016-7606(1988)100<1023:PAPSOL>2.3.CO;2).

- DiPietro, J.A., 2013, Keys to the interpretation of geological history: Landscape evolution in the United States, p. 3–95.
- Eddy, M.P., Clark, K.P., and Polenz, M., 2017, Age and volcanic stratigraphy of the Eocene Siletzia oceanic plateau in Washington and on Vancouver Island: *Lithosphere*, v. 9, p. 652–664, doi:10.1130/L650.1.
- Ehlers, T.A., and Farley, K.A., 2003, Apatite (U–Th)/He thermochronometry: methods and applications to problems in tectonic and surface processes: *Earth and Planetary Science Letters*, v. 206, p. 1–14, doi:10.1016/S0012-821X(02)01069-5.
- Farley, K.A., 2000, Helium diffusion from apatite: General behavior as illustrated by Durango fluorapatite: *Journal of Geophysical Research: Solid Earth*, v. 105, p. 2903–2914, doi:10.1029/1999JB900348.
- Farley, K.A., Shuster, D.L., and Ketcham, R.A., 2011, U and Th zonation in apatite observed by laser ablation ICPMS, and implications for the (U–Th)/He system: *Geochimica et Cosmochimica Acta*, v. 75, p. 4515–4530, doi:10.1016/j.gca.2011.05.020.
- Farley, K.A., Wolf, R.A., and Silver, L.T., 1996, The effects of long alpha-stopping distances on (U–Th)/He ages: *Geochimica et Cosmochimica Acta*, v. 60, p. 4223–4229, doi:10.1016/S0016-7037(96)00193-7.
- Feeley, T.C., 2003, Origin and Tectonic Implications of Across-Strike Geochemical Variations in the Eocene Absaroka Volcanic Province, United States: *The Journal of Geology*, v. 111, p. 329–346, doi:10.1086/373972.
- Feeley, T.C., Cosca, M.A., and Lindsay, C.R., 2002, Petrogenesis and Implications of Calc-Alkaline Cryptic Hybrid Magmas from Washburn Volcano, Absaroka Volcanic Province, USA: *Journal of Petrology*, v. 43, p. 663–703, doi:10.1093/petrology/43.4.663.
- Fernández, J., and Rundle, J.B., 1994, Gravity changes and deformation due to a magmatic intrusion in a two-layered crustal model: *Journal of Geophysical Research: Solid Earth*, v. 99, p. 2737–2746, doi:10.1029/93JB02449.
- Fields, R.W., Rasmussen, D.L., Tabrum, A.R., and Nichols, R., 1985, Cenozoic Rocks of the Intermontane Basins of Western Montana and Eastern Idaho: A Summary: p. 9–36.
- Flowers, R.M., Ketcham, R.A., Shuster, D.L., and Farley, K.A., 2009, Apatite (U–Th)/He thermochronometry using a radiation damage accumulation and annealing model: *Geochimica et Cosmochimica Acta*, v. 73, p. 2347–2365, doi:10.1016/j.gca.2009.01.015.
- Fritz, W.J., and Sears, J.W., 1993, Tectonics of the Yellowstone hotspot wake in, southwestern Montana: *Geology*, v. 21, p. 427–430, doi:10.1130/0091-7613(1993)021<0427:TOTYHW>2.3.CO;2.
- Garber, K.L., Finzel, E.S., and Pearson, D.M., 2020, Provenance of Synorogenic Foreland Basin Strata in Southwestern Montana Requires Revision of Existing Models for Laramide Tectonism: *North American Cordillera: Tectonics*, v. 39, p. e2019TC005944, doi:10.1029/2019TC005944.
- Garihan, J.M., Schmidt, C.J., Young, S.W., and Williams, M.A., 1983, Geology and Recurrent Movement History of the Bismark-Spanish Peaks-Gardiner Fault System, Southwest Montana:, <https://archives.datapages.com/data/rmag/ForelandBasinUp83/garihan.htm> (accessed December 2021).

- Gaschnig, R.M., Vervoort, J.D., Lewis, R.S., and McClelland, W.C., 2010, Migrating magmatism in the northern US Cordillera: in situ U–Pb geochronology of the Idaho batholith: *Contributions to Mineralogy and Petrology*, v. 159, p. 863–883, doi:10.1007/s00410-009-0459-5.
- Gautheron, C., Tassan-Got, L., Barbarand, J., and Pagel, M., 2009, Effect of alpha-damage annealing on apatite (U–Th)/He thermochronology: *Chemical Geology*, v. 266, p. 157–170, doi:10.1016/j.chemgeo.2009.06.001.
- Gilbert, H., 2012, Crustal structure and signatures of recent tectonism as influenced by ancient terranes in the western United States: *Geosphere*, v. 8, p. 141–157, doi:10.1130/GES00720.1.
- Grubbs, F.E., 1969, Procedures for Detecting Outlying Observations in Samples: *Technometrics*, v. 11, p. 1–21, doi:10.1080/00401706.1969.10490657.
- Gunderson, J., 2011, Preliminary Geothermal Map of Montana Using Bottom-Hole Temperature Data: Montana Bureau of Mines and Geology Open-File Report, v. 608, p. 10 p.
- Haller, K.M., Dart, R.L., Machette, M.N., and Stickney, M.C., 2000, Data for Quaternary faults in western Montana: US Geological Survey.
- Haller, K., Wheeler, R., Adema, G., and (Comps.), 2010, Quaternary fault and fold database of the United States: US Geol. Surv.[Available at <http://earthquakes.usgs.gov/hazards/qfaults/>].
- Hanneman, D.L., and Wideman, C.J., 1991, Sequence stratigraphy of Cenozoic continental rocks, southwestern Montana: *GSA Bulletin*, v. 103, p. 1335–1345, doi:10.1130/0016-7606(1991)103<1335:SSOCCR>2.3.CO;2.
- Humphreys, E.D., 1995, Post-Laramide removal of the Farallon slab, western United States: *Geology*, v. 23, p. 987–990, doi:10.1130/0091-7613(1995)023<0987:PLROTF>2.3.CO;2.
- Janecke, S.U., 2007, Cenozoic extensional processes and tectonics in the northern Rocky Mountains: Southwest Montana and eastern Idaho: *Northwest Geology*, v. 36, p. 111–132.
- Janecke, S.U., 1992, Kinematics and timing of three superposed extensional systems, east central Idaho: Evidence for an Eocene tectonic transition: *Tectonics*, v. 11, p. 1121–1138, doi:10.1029/92TC00334.
- Kaempfer, J.M., Guenther, W.R., and Pearson, D.M., 2021, Proterozoic to Phanerozoic Tectonism in Southwestern Montana Basement Ranges Constrained by Low Temperature Thermochronometric Data: *Tectonics*, v. 40, p. e2021TC006744, doi:10.1029/2021TC006744.
- Kasbohm, J., and Schoene, B., 2018, Rapid eruption of the Columbia River flood basalt and correlation with the mid-Miocene climate optimum: *Science Advances*, v. 4, p. eaat8223, doi:10.1126/sciadv.aat8223.
- Kellogg, K.S., and Harlan, S.S., 2007, New ⁴⁰Ar/³⁹Ar age determinations and paleomagnetic results bearing on the tectonic and magmatic history of the northern Madison Range and Madison Valley region, southwestern Montana, U.S.A.: *Rocky Mountain Geology*, v. 42, p. 157–174, doi:10.2113/gsrocky.42.2.157.
- Kellogg, K.S., Schmidt, C.J., and Young, S.W., 1995, Basement and Cover-Rock Deformation During Laramide Contraction in the Northern Madison Range (Montana) and Its Influence on Cenozoic Basin Formation: *AAPG Bulletin*, v. 79, p. 1117–1137, doi:10.1306/8D2B21F5-171E-11D7-8645000102C1865D.

- Kellogg, K.S., and Williams, V.S., 2006, Geologic map of the Ennis 30' x 60' quadrangle, Madison and Gallatin counties, Montana, and Park County, Wyoming: Montana Bureau of Mines and Geology Open-File Report 529, 27 p. p.
- Kellogg, K.S., and Williams, V.S., 1998, Geologic map of the Ennis 30'x 60' quadrangle, Madison and Gallatin Counties, Montana: US Geological Survey.
- Kent-Corson, M.L., Sherman, L.S., Mulch, A., and Chamberlain, C.P., 2006, Cenozoic topographic and climatic response to changing tectonic boundary conditions in Western North America: *Earth and Planetary Science Letters*, v. 252, p. 453–466, doi:10.1016/j.epsl.2006.09.049.
- Ketcham, R.A., 2005, Forward and Inverse Modeling of Low-Temperature Thermochronometry Data: *Reviews in Mineralogy and Geochemistry*, v. 58, p. 275–314, doi:10.2138/rmg.2005.58.11.
- Ketcham, R.A., Gautheron, C., and Tassan-Got, L., 2011, Accounting for long alpha-particle stopping distances in (U–Th–Sm)/He geochronology: Refinement of the baseline case: *Geochimica et Cosmochimica Acta*, v. 75, p. 7779–7791, doi:10.1016/j.gca.2011.10.011.
- Kuenzi, W.D., and Fields, R.W., 1971, Tertiary Stratigraphy, Structure, and Geologic History, Jefferson Basin, Montana: *GSA Bulletin*, v. 82, p. 3373–3394, doi:10.1130/0016-7606(1971)82[3373:TSSAGH]2.0.CO;2.
- Link, P.K., Fanning, C.M., and Beranek, L.P., 2005, Reliability and longitudinal change of detrital-zircon age spectra in the Snake River system, Idaho and Wyoming: An example of reproducing the bumpy barcode: *Sedimentary Geology*, v. 182, p. 101–142, doi:10.1016/j.sedgeo.2005.07.012.
- Locke, W., and Schneider, N., 1990, General geology and geomorphology of the Madison Range and Valley, southwest Montana: *Quaternary Geology of the Western Madison Range, Madison Valley, Tobacco Root Range, and Jefferson Valley Rocky Mountain Friends of the Pleistocene*, p. 1–23.
- McQuarrie, N., and Rodgers, D.W., 1998, Subsidence of a volcanic basin by flexure and lower crustal flow: The eastern Snake River Plain, Idaho: *Tectonics*, v. 17, p. 203–220, doi:10.1029/97TC03762.
- Miller, R.B., Gordon, S.M., Bowring, S., Doran, B., McLean, N., Michels, Z., Shea, E., and Whitney, D.L., 2016, Linking deep and shallow crustal processes during regional transtension in an exhumed continental arc, North Cascades, northwestern Cordillera (USA): *Geosphere*, v. 12, p. 900–924, doi:10.1130/GES01262.1.
- Monroe, S., 1981, Late Oligocene-early Miocene facies and lacustrine sedimentation, upper Ruby River basin, southwestern Montana: *Journal of Sedimentary Research*, v. 51, p. 939–951, doi:10.1306/212F7DE7-2B24-11D7-8648000102C1865D.
- Morgan, W.J., 1972, Deep Mantle Convection Plumes and Plate Motions 1: *AAPG Bulletin*, v. 56, p. 203–213, doi:10.1306/819A3E50-16C5-11D7-8645000102C1865D.
- Murphy, B.J., Oppliger, G.L., Brimhall, G.H., Jr, and Hynes, A., 1998, Plume-modified orogeny: An example from the western United States: *Geology*, v. 26, p. 731–734, doi:10.1130/0091-7613(1998)026<0731:PMOAEF>2.3.CO;2.

- O'Neill, J.M., Lonn, J.D., Lageson, D.R., and Kunk, M.J., 2004, Early Tertiary Anaconda Metamorphic Core Complex, southwestern Montana: *Canadian Journal of Earth Sciences*, v. 41, p. 63–72, doi:10.1139/e03-086.
- Pardee, J.T., 1950, Late Cenozoic block faulting in western Montana: *GSA Bulletin*, v. 61, p. 359–406, doi:10.1130/0016-7606(1950)61[359:LCBFIW]2.0.CO;2.
- Pierce, K.L., Licciardi, J.M., Krause, T.R., and Whitlock, C., 2014, Glacial and Quaternary geology of the northern Yellowstone area, Montana and Wyoming: *Exploring the Northern Rocky Mountains*, v. 37, p. 189–203.
- Pierce, K.L., and Morgan, L.A., 2009, Is the track of the Yellowstone hotspot driven by a deep mantle plume? — Review of volcanism, faulting, and uplift in light of new data: *Journal of Volcanology and Geothermal Research*, v. 188, p. 1–25, doi:10.1016/j.jvolgeores.2009.07.009.
- Reiners, P.W., and Farley, K.A., 2001, Influence of crystal size on apatite (U–Th)/He thermochronology: an example from the Bighorn Mountains, Wyoming: *Earth and Planetary Science Letters*, v. 188, p. 413–420, doi:10.1016/S0012-821X(01)00341-7.
- Robinson, G.D., 1961, Origin and Development of the Three Forks Basin, Montana: *GSA Bulletin*, v. 72, p. 1003–1013, doi:10.1130/0016-7606(1961)72[1003:OADOTT]2.0.CO;2.
- Robinson, G.D., and Barnett, H.F., 1963, *Geology of the Three Forks Quadrangle, Montana, with sections on petrography of igneous rocks*: United States Government Printing Office.
- Rodgers, D.W., Hackett, W.R., and Ore, H.T., 1990, Extension of the Yellowstone plateau, eastern Snake River Plain, and Owyhee plateau: *Geology*, v. 18, p. 1138–1141, doi:10.1130/0091-7613(1990)018<1138:EOTYPE>2.3.CO;2.
- Rodgers, D.W., Ore, H.T., Bobo, R.T., McQuarrie, N., Zentner, N., Bonnicksen, B., White, C., and McCurry, M., 2002, Extension and subsidence of the eastern Snake River Plain, Idaho: *Tectonic and Magmatic Evolution of the Snake River Plain Volcanic Province*: Idaho Geological Survey Bulletin, v. 30, p. 121–155.
- Schofield, J.D., 1981, A structure of the Centennial and Madison Valleys based on gravitational interpretation: p. 275–284.
- Schwartz, T.M., Methner, K., Mulch, A., Graham, S.A., and Chamberlain, C.P., 2019, Paleogene topographic and climatic evolution of the Northern Rocky Mountains from integrated sedimentary and isotopic data: *GSA Bulletin*, v. 131, p. 1203–1223, doi:10.1130/B32068.1.
- Schwartz, T.M., and Schwartz, R.K., 2013, Paleogene postcompressional intermontane basin evolution along the frontal Cordilleran fold-and-thrust belt of southwestern Montana: *GSA Bulletin*, v. 125, p. 961–984, doi:10.1130/B30766.1.
- Sears, J.W., Hendrix, M.S., Thomas, R.C., and Fritz, W.J., 2009, Stratigraphic record of the Yellowstone hotspot track, Neogene Sixmile Creek Formation grabens, southwest Montana: *Journal of Volcanology and Geothermal Research*, v. 188, p. 250–259.
- Sears, J.W., and Ryan, P.C., 2003, Cenozoic Evolution of the Montana Cordillera: Evidence From Paleovalleys: p. 289–301.
- Sears, J.W., and Thomas, R.C., 2007, Extraordinary middle Miocene crustal disturbance in southwest Montana: birth record of the Yellowstone hot spot, *in* Introduction to the Geology of the Dillon area: Northwest Geology: Dillon Field Conference, v. 36, p. 133–142.

- Shuster, D.L., Flowers, R.M., and Farley, K.A., 2006, The influence of natural radiation damage on helium diffusion kinetics in apatite: *Earth and Planetary Science Letters*, v. 249, p. 148–161, doi:10.1016/j.epsl.2006.07.028.
- Smith, R.B., Jordan, M., Steinberger, B., Puskas, C.M., Farrell, J., Waite, G.P., Husen, S., Chang, W.-L., and O’Connell, R., 2009, Geodynamics of the Yellowstone hotspot and mantle plume: Seismic and GPS imaging, kinematics, and mantle flow: *Journal of Volcanology and Geothermal Research*, v. 188, p. 26–56, doi:10.1016/j.jvolgeores.2009.08.020.
- Sonder, L.J., and Jones, C.H., 1999, Western United States Extension: How the West was Widened: *Annual Review of Earth and Planetary Sciences*, v. 27, p. 417–462, doi:10.1146/annurev.earth.27.1.417.
- Spiegel, C., Kohn, B., Belton, D., Berner, Z., and Gleadow, A., 2009, Apatite (U–Th–Sm)/He thermochronology of rapidly cooled samples: The effect of He implantation: *Earth and Planetary Science Letters*, v. 285, p. 105–114, doi:10.1016/j.epsl.2009.05.045.
- Staisch, L.M., O’Connor, J.E., Cannon, C.M., Holm-Denoma, C., Link, P.K., Lasher, J., and Alexander, J.A., 2021, Major reorganization of the Snake River modulated by passage of the Yellowstone Hotspot: *GSA Bulletin*, doi:10.1130/B36174.1.
- Suppe, J., Powell, C., and Berry, R., 1975, Regional topography, seismicity, Quaternary volcanism, and the present-day tectonics of the western United States: *Am. J. Sci*, v. 275, p. 397–436.
- Tranel, L.M., Spotila, J.A., Kowalewski, M.J., and Waller, C.M., 2011, Spatial variation of erosion in a small, glaciated basin in the Teton Range, Wyoming, based on detrital apatite (U–Th)/He thermochronology: *Basin Research*, v. 23, p. 571–590, doi:10.1111/j.1365-2117.2011.00502.x.
- Trimble, A.B., and Smith, R.B., 1975, Seismicity and contemporary tectonics of the Hebgen Lake–Yellowstone Park Region: *Journal of Geophysical Research (1896-1977)*, v. 80, p. 733–741, doi:10.1029/JB080i005p00733.
- Tysdal, R.G., Marvin, R.F., and Dewitt, E., 1986, Late Cretaceous stratigraphy, deformation, and intrusion in the Madison Range of southwestern Montana: *GSA Bulletin*, v. 97, p. 859–868, doi:10.1130/0016-7606(1986)97<859:LCSDAI>2.0.CO;2.
- Van Wijk, J., Axen, G., Abera, Y., and Yao, S., 2016, Surface uplift due to thermal expansion around the Socorro magma body: Preliminary results, *in* *New Mexico Geological Society Guidebook, 67th Field Conference*, p. 217–223.
- Vermeesch, P., Resentini, A., and Garzanti, E., 2016, An R package for statistical provenance analysis: *Sedimentary Geology*, v. 336, p. 14–25, doi:10.1016/j.sedgeo.2016.01.009.
- Vermeesch, P., Seward, D., Latkoczy, C., Wipf, M., Günther, D., and Baur, H., 2007, α -Emitting mineral inclusions in apatite, their effect on (U–Th)/He ages, and how to reduce it: *Geochimica et Cosmochimica Acta*, v. 71, p. 1737–1746, doi:10.1016/j.gca.2006.09.020.
- Vogl, J.J., Min, K., Carmenate, A., Foster, D.A., and Marsellos, A., 2014, Miocene regional hotspot-related uplift, exhumation, and extension north of the Snake River Plain: Evidence from apatite (U–Th)/He thermochronology: *Lithosphere*, v. 6, p. 108–123, doi:10.1130/L308.1.
- Vuke, S., 2013, *Geologic Map of the Fan Mountain, Lone Mountain & Gallatin Peak 7.5’ Quadrangles, Madison Range, Madison & Gallatin Counties, Montana*: Montana Bureau of Mines and Geology.

- Vuke, S.M., Lonn, J.D., Berg, R.B., and Kellogg, K.S., 2002, Preliminary geologic map of the Bozeman 30' \times 60 quadrangle, southwestern Montana: MBMG Open File No, v. 469.
- Waschbusch, P.J., and McNutt, M.K., 1994, Yellowstone: A continental midplate (hot spot) swell: *Geophysical Research Letters*, v. 21, p. 1703–1706, doi:10.1029/94GL00429.
- Wegmann, K.W. et al., 2007, Position of the Snake River watershed divide as an indicator of geodynamic processes in the greater Yellowstone region, western North America: *Geosphere*, v. 3, p. 272–281, doi:10.1130/GES00083.1.
- Wolf, R.A., Farley, K.A., and Kass, D.M., 1998, Modeling of the temperature sensitivity of the apatite (U–Th)/He thermochronometer: *Chemical Geology*, v. 148, p. 105–114, doi:10.1016/S0009-2541(98)00024-2.
- Wolf, R.A., Farley, K.A., and Silver, L.T., 1996, Helium diffusion and low-temperature thermochronometry of apatite: *Geochimica et Cosmochimica Acta*, v. 60, p. 4231–4240, doi:10.1016/S0016-7037(96)00192-5.
- Yonkee, W.A., and Weil, A.B., 2015, Tectonic evolution of the Sevier and Laramide belts within the North American Cordillera orogenic system: *Earth-Science Reviews*, v. 150, p. 531–593, doi:10.1016/j.earscirev.2015.08.001.